

DiskANN++: Efficient Page-based Search over Isomorphic Mapped Graph Index using Query-sensitivity Entry Vertex

Jiongkang Ni¹, Xiaoliang Xu^{1*}, Yuxiang Wang¹, Can Li¹, Jiajie Yao², Shihai Xiao², Xuecang Zhang²

¹Hangzhou Dianzi University, China, ²Huawei Technologies Co., Ltd, China

{hananoyuuki,xxl,lsswyx,lic}@hdu.edu.cn,{yaojiajie1,xiaoshihai,zhangxuecang}@huawei.com

ABSTRACT

Given a vector dataset \mathcal{X} and a query vector \vec{x}_q , graph-based Approximate Nearest Neighbor Search (ANNS) aims to build a graph index G and approximately return vectors with minimum distances to \vec{x}_q by searching over G . The main drawback of graph-based ANNS is that a graph index would be too large to fit into the memory especially for a large-scale \mathcal{X} . To solve this, a Product Quantization (PQ)-based hybrid method called DiskANN is proposed to store a low-dimensional PQ index in memory and retain a graph index in SSD, thus reducing memory overhead while ensuring a high search accuracy. However, it suffers from two I/O issues that significantly affect the overall efficiency: (1) long routing path from an entry vertex to the query's neighborhood that results in large number of I/O requests and (2) redundant I/O requests during the routing process. We propose an optimized DiskANN++ to overcome above issues. Specifically, for the first issue, we present a *query-sensitive entry vertex selection strategy* to replace DiskANN's static graph-central entry vertex by a dynamically determined entry vertex that is close to the query. For the second I/O issue, we present an *isomorphic mapping on DiskANN's graph index to optimize the SSD layout* and propose an *asynchronously optimized Pagesearch based on the optimized SSD layout* as an alternative to DiskANN's beam-search. Comprehensive experimental studies on eight real-world datasets demonstrate our DiskANN++'s superiority on efficiency. We achieve a notable 1.5 X to 2.2 X improvement on QPS compared to DiskANN, given the same accuracy constraint.

PVLDB Reference Format:

Jiongkang Ni¹, Xiaoliang Xu^{1*}, Yuxiang Wang¹, Can Li¹, Jiajie Yao², Shihai Xiao², Xuecang Zhang². DiskANN++: Efficient Page-based Search over Isomorphic Mapped Graph Index using Query-sensitivity Entry Vertex. PVLDB, 17(1): XXX-XXX, 2023.

doi:XX.XX/XXX.XX

PVLDB Artifact Availability:

The source code, data, and/or other artifacts have been made available at https://anonymous.4open.science/r/DiskANN_plusplus-5533.

1 INTRODUCTION

Approximate Nearest Neighbor Search (ANNS) [7, 27] has been widely studied recently, which is fundamental for many real-world

This work is licensed under the Creative Commons BY-NC-ND 4.0 International License. Visit <https://creativecommons.org/licenses/by-nc-nd/4.0/> to view a copy of this license. For any use beyond those covered by this license, obtain permission by emailing info@vldb.org. Copyright is held by the owner/author(s). Publication rights licensed to the VLDB Endowment.

Proceedings of the VLDB Endowment, Vol. 17, No. 1 ISSN 2150-8097.

doi:XX.XX/XXX.XX

* Corresponding author: xxl@hdu.edu.cn

applications, such as recommendation systems [44, 53], information retrieval [17, 58], data mining [1, 10], and pattern recognition [13, 65]. Given a vector dataset \mathcal{X} and a query vector $\vec{x}_q \in \mathcal{X}$, ANNS aims to return approximate nearest neighbors to \vec{x}_q from \mathcal{X} with minimum distance [52]. ANNS is generally categorized as four types: *hashing-based* [21, 23], *tree-based* [6, 46], *quantization-based* [12, 31], and *graph-based* [19, 38] methods. Among them, graph-based ANNS attracts more attention and has been regarded as the most promising one due to its impressive efficiency and effectiveness over large-scale datasets [5, 8, 11, 19, 24, 40, 45, 52].

Graph-based ANNS uses a graph index (e.g., NSG [19], HNSW [38], etc.) maintained in the memory to facilitate approximate nearest neighbors retrieval. Each vertex in a graph index represents a vector in \mathcal{X} , and an edge between two vertices defines a neighbor relationship. During the retrieval phase, a graph routing over the graph index is conducted, starting from an entry vertex and iteratively exploring the graph index along the vertices that can guide the search closer to the query \vec{x}_q until it converges [38]. *The main limitation of graph-based ANNS comes from the heavyweight memory overhead of a graph index.* The memory overhead significantly increases as \mathcal{X} increases, e.g., using HNSW as a graph index for a billion-scale \mathcal{X} in 128 dimensions would consume around 800 GB memory, which largely exceeds the RAM capacity on a workstation.

Existing solutions. Many efforts have been made to alleviate the memory issue of graph-based ANNS for large-scale datasets. We briefly discuss some representative methods as follows. *GRIP* [64] reduces the memory consumption of a graph index by replacing high-dimensional vectors with lower-dimensional ones through compression. *SPANN* [11] clusters on the dataset and uses the centroids to construct a spatial partitioning tree (SPT) that resides in memory. High-dimensional vectors within each cluster are stored on SSD. The search algorithm locates the nearest centroids to the query from SPT, then loads the corresponding clusters from SSD for identifying the top- k nearest neighbors to the query. *BBANN* [47] conducts balanced clustering on the dataset and uses the clustered centroids to build a graph index maintained in memory. High-dimensional vectors within each cluster are stored on SSD. The search algorithm firstly routes on the graph index in memory to find the nearest centroid to the query. Then it conducts a BFS with limited hops to extend candidate centroids. Finally, it loads all corresponding clusters from SSD to identify the top- k nearest neighbors.

The search accuracy of above methods is significantly affected by the compressed vectors or low-quality graph index of clustered centroids, resulting in a noticeable accuracy loss, e.g., the maximum recall@100 reduces from 95% to 87% for SPANN at the same latency.

DiskANN [29]. This motivates a state-of-the-art work DiskANN, a Product Quantization (PQ)-based hybrid (memory+SSD) method that aims to reduce memory overhead while ensuring a high search

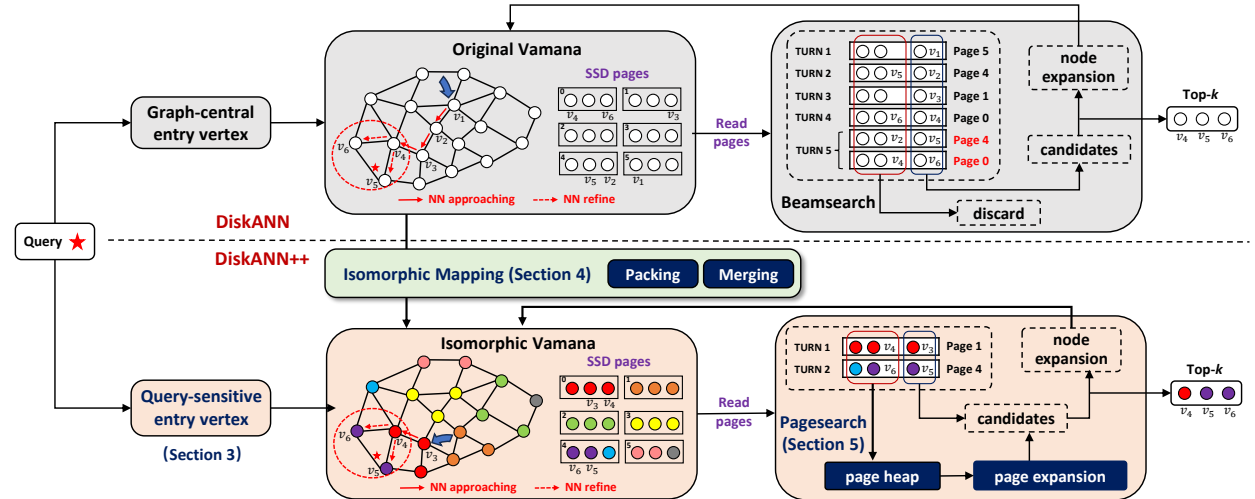


Figure 1: Search examples on DiskANN (top) and DiskANN++ (bottom), given the same query vertex and the Vamana graph index with the same topological structure but different SSD layout.

accuracy. It first conducts PQ for original high-dimensional vectors to obtain the quantized low-dimensional vectors, then stores a PQ index for quantized vectors in memory and a graph index for original vectors in SSD. PQ index serves for lossy distance calculations, based on which initial candidate neighbors are provided. Graph index serves for re-ranking candidate neighbors based on original vectors, which can be viewed as a post-verification of lossy distances, so as to ensure the candidates’ quality and enhance the search accuracy. We refer readers to [29] and §2 for more details. DiskANN has been widely deployed in the industry such as Bing search of Microsoft [63] and many follow-up works present variants of DiskANN to support their own scenarios, e.g., Filter-DiskANN for filtered search [22], OOD-DiskANN for cross-modal search [28], and Fresh-DiskANN for streaming search [48]. Although DiskANN and its variants achieve a good performance on both memory overhead and search accuracy, they all ignore the important I/O issue (frequent SSD I/O requests for candidates re-ranking) that significantly affect the overall queries per second (QPS). In general, the latency of accessing SSD is 10X+ greater than that of accessing main memory, the more the SSD I/O requests, the more the time for DiskANN. We next briefly discuss the I/O issue of DiskANN.

I/O issue of DiskANN. Figure 1 (top) illustrates the search process of DiskANN on the Vamana graph index maintained in SSD. Vertices in Vamana are assigned into SSD pages in a round-robin manner, e.g., 6 pages are used to record 18 vertices in this example. Given a query vertex indicated by a red star, DiskANN adopts *beamsearch* (discussed later in §2) to retrieve the top- k results. It starts from the static entry vertex (i.e., the central vertex of a graph index) to explore a routing path towarding to query’s neighborhood. We call this the *nearest neighbor approaching* (NN approaching) phase [59]. DiskANN first reads SSD to get the Page-5 involving the entry vertex v_1 , then takes v_1 as candidate for node expansion and discard the other nodes. In the step of *node expansion*, DiskANN computes the distances between candidates’ neighbors to query and requests SSD Page-4 to obtain the closest vertex v_2 . It repeats until the search locates in the neighborhood of query (indicated by a red dashed circle). NN approaching stops when v_4 is explored. Next, DiskANN

goes into the phase of *nearest neighbor refine* (NN refine) to find the top- k nearest neighbors to query via a nearly a brute-force vertex traversal in query’s neighborhood. Both Page-0 and Page-4 are requested to obtain v_4 ’s two neighbors v_5, v_6 .

We summarize that the I/O issue of DiskANN is two-fold: (1) *Long routing path in NN approaching phase* and (2) *Redundant I/O requests in NN refine phase*. For (1), since DiskANN takes the graph-central vertex as a static entry vertex for all queries, it would result in a long routing path in NN approaching phase, when the query is far away from the entry vertex. In above example, it needs 3 hops from v_1 to query’s neighborhood, yielding 4 SSD I/O requests out of the total 6 requests. In practice, queries often arrive randomly, which leads to a large number of long routing paths, so that affecting the overall efficiency. For (2), since DiskANN adopts a random SSD layout, it would result in redundant I/O requests in NN refine phase, when vertices on the same SSD page have less closeness in the graph index. In this example, each accessed page only involves one useful vertex for beamsearch, thus reducing the data value of each I/O request and leading two redundant I/O requests of Page-0 and Page-4 in the NN refine phase. Actually, they have been accessed in NN approaching phase, however, DiskANN does not know they would be required later and directly discard them as instead.

The aforementioned I/O issue inspires our study in this paper to shorten the routing path and improve the effectiveness of each I/O request (i.e., making an I/O request carry more useful vertices that can facilitate search process), so that significantly reduce the total number of I/O requests and increase the overall QPS of DiskANN.

Our solution. We next briefly introduce our solution as follows. (1) **Query-sensitive entry vertex selection (§3).** For the long routing path problem, we present a query-sensitive entry vertex selection strategy to dynamically determine the entry vertex in run-time instead of the original static graph-central entry vertex (§3.1). Given a vector dataset \mathcal{X} and a Vamana graph index built for \mathcal{X} , we first cluster the dataset to acquire N_{cluster} centroids, then we take each centroid as a query to perform ANNS on Vamana to find its top-1 nearest vertex, and finally we add all the N_{cluster} nearest vertices and the graph-central vertex into an *entry vertex candidate list*. For

each incoming query \vec{x}_q , we linearly scan the candidate list and employ the nearest vertex to \vec{x}_q as the entry vertex. In Figure 1 (bottom), we may select v_3 as the entry vertex, leading a 1-hop routing path to query’s neighborhood. In §3.2, we leverage the monotonicity of MSNET [14, 66] to theoretically prove that using query-sensitive entry vertex would result in a shorter routing path than that of static graph-central entry vertex. In general, the shorter routing path usually indicates the less SSD I/O requests.

We next show our solutions to redundant I/O issue: *isomorphic mapping of graph index* and *page-level optimization to beamsearch*.

(2) Isomorphic mapping of graph index (§4). We propose an *isomorphic mapping on Vamana* to optimize the SSD layout. Specifically, we first apply an injective mapping via *star packing* [9] on the original Vamana. It effectively assigns the vertices with great closeness into the same SSD page, so that increasing the data value of each individual I/O request. Then, we apply *bin packing* based on *First Fit Decreasing* (FFD) to make the injective mapping also surjective, i.e., converting the injection to bijection (or isomorphic mapping), thereby ensuring that the original graph’s topology and addressing mode are preserved in the new SSD layout. In Figure 1 (bottom), we show the refined SSD layout with coloured vertices. Note that, vertices that are close to each other are likely to be assigned to the same SSD page. Suppose we start search from v_3 and v_4 is the next-hop vertex of graph routing. Since v_4 and v_3 are retained in the same SSD page, we only need one SSD I/O request for Page-1 to access them simultaneously. Similarly, we only require additional one SSD I/O request for Page-4 to access v_5 and v_6 simultaneously.

(3) Page-level optimizations to beamsearch (§5). On the basis of the refined SSD layout via isomorphic mapping on Vamana, we present a new search algorithm with page-level optimizations called *Page-search* as an alternative to beamsearch. The basic idea is to harness the idle CPU resources during SSD I/O requests to further mitigating the search latency. Since we apply isomorphic mapping on Vamana, each page contains more valuable vertices that would be used for the following search process. So, we first design a novel component called *page heap* to asynchronously cache the valuable vertices from previously accessed pages. Next, we expand search from the cached valuable vertices via an asynchronous *page expansion* using the idle CPU resources while waiting the results of SSD I/O requests. The vertices obtained by page expansions would be added into the global candidates for next step of node expansion. Node expansion is a key operation of beamsearch and more details are provided in §2. In a nutshell, the page expansion is a complement to node expansion by providing more useful candidates from the previously accessed pages. It is a concurrent operation with SSD I/O requests without introducing extra latency.

Figure 2 shows an ablation analysis of DiskANN using beamsearch and pagesearch with static entry vertex and query-sensitive entry vertex, respectively, given the same queries under the same recall@100 of 99%. The X-axis is the sequence of I/O requests, while Y-axis shows the average vector distance over all accessed vertices in an I/O request to the query. We use the blue (red) points in plot to represent the I/O requests in NN approaching (NN refine) phase. As more I/O requests are performed, the search is getting more closer to the query. Figure 2 (a) and (b) show results using beamsearch with different entry vertex strategies, we found that using

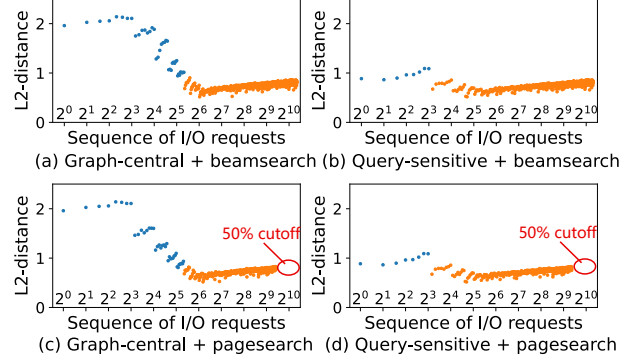


Figure 2: Comparison of our pagesearch and original beamsearch with different entry vertex strategies (deep100M).

query-sensitive entry vertex would significantly reduce the SSD I/O requests in NN approaching phase from 32 to 8. Figure 2 (a) and (c) show results using beamsearch and pagesearch with the same static entry vertex, we found that the SSD I/O requests in NN refine phase are reduced by at least 50%. Figure 2 (d) shows the results using pagesearch with query-sensitive entry vertex, i.e., our DiskANN++. Comparing with DiskANN (Figure 2 (a)), our solution achieves a better I/O efficiency in both two phases (nearly 0.5 X less SSD I/O requests), leading to a 2 X improvement on QPS.

Contributions. Our contributions can be concluded as follows.

- (1) We propose a query-sensitive entry vertex selection strategy to determine entry vertex dynamically (§3), which addresses the I/O issue during NN approaching phase caused by long routing path from a far away entry vertex to the query.
- (2) We present an isomorphic mapping on Vamana in §4, which assigns vertices with great closeness to the same SSD page so that refine the SSD layout, thus effectively enhancing the data value of each individual SSD I/O request.
- (3) We design a novel search algorithm called Pagesearch with page-level optimizations based on the refined SSD layout (§5), which utilizes idle CPU resources to update global candidates with more valuable vertices, thereby reducing the redundant SSD I/O request and accelerating the convergence.
- (4) Extensive experiments on public and commercial datasets of different types and scales, under diverse hardware resource configurations, show that our solution achieves a notable QPS improvement ranging from 1.5 X to 2.2 X.

2 PRELIMINARY

Fundamental definitions. We start with several fundamental definitions and two widely used metrics for evaluating ANNS.

DEFINITION 1. ANNS [52]. Given a vector dataset \mathcal{X} , a query vector \vec{x}_q , and a parameter $\epsilon > 0$, the goal of ANNS is to find the top- k vectors $\{\vec{x}_1, \dots, \vec{x}_k\}$ from \mathcal{X} that are approximate nearest neighbors to \vec{x}_q . We say a vector $\vec{x}_i \in \mathcal{X}$ is an approximate nearest neighbor to \vec{x}_q if $\delta(\vec{x}_i, \vec{x}_q) \leq (1 + \epsilon) \cdot \delta(\vec{x}_i^*, \vec{x}_q)$, where $\vec{x}_i^* \in \mathcal{X}$ is the i -th nearest neighbor vector of \vec{x}_q (i.e., the i -th ground-truth vector) and ϵ is an relaxation parameter that controls the top- k results’ quality.

DEFINITION 2. Graph index. Given a vector dataset \mathcal{X} and a user-defined non-negative distance threshold $\bar{\delta}$, we define the graph index of \mathcal{X} w.r.t. $\bar{\delta}$ as a graph $G = (V, E)$ with the vertex set V and edge set E . (1) There is a bijection $\phi : \mathcal{X} \rightarrow V$ so that $\forall \vec{x}_v \in \mathcal{X}, \exists v \in V$ satisfying $v = \phi(\vec{x}_v)$, or we say each vertex $v \in V$ corresponds to a vector $\vec{x}_v \in \mathcal{X}$. (2) For any two vertices $v_i, v_j \in V$ ($i \neq j$), there exists an edge $e(v_i, v_j) \in E$ iff $\delta(\vec{x}_{v_i}, \vec{x}_{v_j}) < \bar{\delta}$.

DEFINITION 3. Recall@k. Given a query vector \vec{x}_q , we use \mathcal{R}^* to record the ground-truth nearest neighbors with k vectors from the vector dataset \mathcal{X} and we use \mathcal{R} to record k approximate nearest neighbors returned by ANNS. Then we define the Recall@ k as follows.

$$\text{Recall}@k = \frac{|\mathcal{R}^* \cap \mathcal{R}|}{|\mathcal{R}^*|} = \frac{|\mathcal{R}^* \cap \mathcal{R}|}{k} \quad (1)$$

DEFINITION 4. Queries Per Second (QPS). QPS is a metric that indicates the number of queries that an ANNS method can handle per second. Suppose an ANNS method processes N_q queries within a period of T seconds, then we have $\text{QPS} = N_q/T$.

In practice, the higher Recall@ k and QPS always mean a better search accuracy and efficiency of ANNS, respectively.

Briefly introduction to DiskANN. We briefly introduce the SSD layout of the graph index and beamsearch used in DiskANN, which is important for understanding our proposed solutions in §4-5.

Original SSD layout. DiskANN employs a straightforward method to store the graph index $G = (V, E)$ for a vector dataset \mathcal{X} .

DEFINITION 5. Data block. Given a vertex $v \in V$, we define the data block of v as $b_v = \langle \vec{x}_v, N(v) \rangle$, which is the basic unit for SSD storage. (1) $\vec{x}_v \in \mathcal{X}$ is the corresponding vector of v . (2) $N(v)$ recodes the identities of v 's neighbors in G . (3) We use v to indicate the identity of the data block b_v , denoted by $b_v.\text{ID} = v$.

Given data blocks of all $|V|$ vertices, DiskANN stores them to SSD pages in a round-robin manner with page alignment. We use $L = \{P_1, \dots, P_n\}$ to denote the SSD layout with n pages and each page $P = \{b_{v_1}, \dots, b_{v_b}\}$ contains b data blocks. For facilitating discussion, in the rest of this paper, we use $L.\text{IDs} = \{P_1.\text{IDs}, \dots, P_n.\text{IDs}\}$ to denote the logic view of a layout that only consists of the identities of all data blocks, where $P.\text{IDs} = \{v_1, \dots, v_b\}$.

Beamsearch. Beamsearch is the core search algorithm of DiskANN, but the details are ignored in [29]. Here, we show its procedure in Algorithm 1. Given a SSD-resident graph index $G = (V, E)$ of the vector dataset \mathcal{X} , query vector \vec{x}_q , beam size B , search width L_s , and the size k of top- k results, beamsearch does the followings. (1) It starts search from a static graph-central entry vertex $v_e \in V$ with a candidate set $C = \{v_e\}$ and an empty top- k results set \mathcal{R} (lines 1-3). It's worth mentioning that vertices in C are ranked in ascending ordered of their PQ distances to \vec{x}_q using the memory-resident quantized vectors. While the vertices in \mathcal{R} are ranked in ascending ordered of their full distances to \vec{x}_q using the SSD-resident original vectors. (2) It chooses the unvisited top- B vertices (at most B) from the candidate set C , denoted by \mathcal{F} and creates page placeholders P_j into \mathcal{P} to register read requests for them (line 6-10). Finally, it reads all required pages from SSD (line 11). (3) It use all unvisited vertices from \mathcal{F} to perform node expansion (lines 12-15). The node expansion phase mainly consist of B times NeighborExpansion

Algorithm 1: Beamsearch(G, \vec{x}_q, B, L_s, k)

```

Input: graph index  $G$ , query  $\vec{x}_q$ , beam size  $B$ , search width  $L_s$ , size  $k$  of top- $k$ 
Output: approximate nearest top- $k$  neighbors  $\mathcal{R}$  to  $\vec{x}_q$ 
// Initialization: lines 1-3
1  $v_e \leftarrow$  the central vertex of  $G$ ; /* static entry vertex */
2  $C \leftarrow \{v_e\}$ ; /* candidate set initialized as  $\{v_e\}$  */
3  $\mathcal{R} \leftarrow \emptyset$ ; /* top- $k$  results initialized as empty */
4 do
5    $\mathcal{F} \leftarrow$  top- $B$  unvisited vertices from  $C$  for expansion ;
  // prepare SSD I/O requests: line 6-10
6    $\mathcal{P} \leftarrow \emptyset$ ; /* page placeholders initialized as empty */
7   for  $v_i \in \mathcal{F}$  do
8      $P_j \leftarrow$  register read for page containing  $b_{v_i}$  ;
9      $\mathcal{P} \leftarrow \mathcal{P} \cup P_j$  ;
10  end
11 // SSD I/O requests: line 11
12  read all required pages in  $\mathcal{P}$  from SSD ;
13 // Node expansion: lines 12-15
14  for  $v_i \in \mathcal{F}$  do
15     $b_{v_i} = \langle \vec{x}_{v_i}, N(v_i) \rangle \leftarrow$  obtained from  $\mathcal{P}$  ;
    NeighborExpansion( $\vec{x}_q, b_{v_i}, C, \mathcal{R}, L_s, k$ ) ;
16  end
17 while  $\mathcal{F} \neq \emptyset$  ;
18 return  $\mathcal{R}$ ;
```

Algorithm 2: NeighborExpansion($\vec{x}_q, b_v, C, \mathcal{R}, L_s, k$)

```

Input: query  $\vec{x}_q$ , data block  $b_v = \langle \vec{x}_v, N(v) \rangle$ , PQ distance based
ordered set  $C$ , full distance based ordered set  $\mathcal{R}$ , search
width  $L_s$ , size  $k$  of top- $k$ 
1  $C \leftarrow C \cup N(v)$ ; /* sort  $C$  by PQ distance to  $\vec{x}_q$  */
2 while  $|C| > L_s$  do
3   | pop back from  $C$  ;
4 end
5  $\mathcal{R} \leftarrow \mathcal{R} \cup \{\vec{x}_v\}$ ; /* sort  $\mathcal{R}$  by full distance to  $\vec{x}_q$  */
6 while  $|\mathcal{R}| > k$  do
7   | pop back from  $\mathcal{R}$  ;
8 end
```

(Algorithm 2) operations. NeighborExpansion uses a data block $b_v = \langle \vec{x}_v, N(v) \rangle$ to update the candidate set C and top- k results set \mathcal{R} . It updates C with the neighbors $N(v)$ in ascending order of PQ distance to \vec{x}_q and ensure C 's length $\leq L_s$. Then, it updates the top- k results set \mathcal{R} with \vec{x}_v in ascending order of full distance to \vec{x}_q and ensure \mathcal{R} 's length $\leq k$. The re-ranking operation to \mathcal{R} is the key to guarantee the search accuracy. (4) It repeats above until no new vertex is visited and returns \mathcal{R} as the top- k results.

Problem definition. Given a vector dataset \mathcal{X} , a memory constraint M , a graph index G built for \mathcal{X} (i.e., Vamana for DiskANN), and a query vector \vec{x}_q , DiskANN aims maintain a PQ index within M size in memory and leverage the SSD-resident G to return the top- k approximate nearest neighbors to \vec{x}_q with a high Recall@ k .

On this basis, our goal is summarized as: Given the conditions unchanged, we aim to design a refined SSD layout of graph index and a new search algorithm based on such layout, for retrieving the top- k results having the same Recall@ k as DiskANN, while improving the overall QPS by reducing the number of SSD I/O requests, i.e., we expect to increase QPS without sacrificing accuracy.

3 QUERY-SENSITIVE ENTRY VERTEX

To solve the first I/O issue of DiskANN, i.e., the long routing path from an entry vertex to a query \vec{x}_q 's neighborhood, we present a

query-sensitive entry vertex selection strategy as an instead of the static graph-central entry vertex used in DiskANN.

3.1 Method Overview

The basic idea is concluded as: we first prepare a set of representative entry vertex candidates offline and then select an appropriate entry vertex from above candidates for each incoming query online.

Offline candidate entry vertices generation. Given a vector dataset \mathcal{X} and the Vamana graph index G of \mathcal{X} , we generate the entry vertex candidates as follows. First, we employ the *mini-batch-kmeans* [41] to cluster \mathcal{X} into N_{cluster} clusters $\{c_1, \dots, c_{N_{\text{cluster}}}\}$, this step is used to divide the original vector space logically. Second, we take each c_i 's centroid as an input query \vec{x}_q to find its top-1 nearest neighbor from G . Finally, we record all the nearest neighbors for N_{cluster} centroids in a linear table as the entry vertex candidates.

Online entry vertex selection. Since each candidate is a representative vertex of a partition of \mathcal{X} , it's reasonable to take it as the entry vertex when the incoming query locates in its corresponding partition. To this end, given the candidate entry vertices and a query vertex \vec{x}_q , we first compute the distance of each candidate to \vec{x}_q , then we select the one with the closest distance as the entry vertex.

We next theoretically analyze the effectiveness of query-sensitivity entry vertex selection using the monotonicity of Monotonic Search Network (MSNET) [14, 66] (§3.2) and discuss the complexity (§3.3).

3.2 Theoretical Analysis of Effectiveness

In this section, we prove that using our query-sensitivity entry vertex can provide a tighter upper bound on the length of a routing path required for the search to converge. Since the graph index of DiskANN, i.e., Vamana, is developed based on the fundamental graph called Monotonic Search Network (MSNET) [29], similar to [19], we leverage MSNET's monotonicity to complete our analysis.

DEFINITION 6 (MONOTONIC PATH). *Given a graph index $G(V, E)$ built for a vector dataset \mathcal{X} . Let $v_s, v_t \in V$, an l -hop path $\mathcal{P}(v_s, v_t)$ from v_s to v_t is a Monotonic Path, iff $\exists v_1, \dots, v_{l+1} \in V$ ($v_1 = v_s, v_{l+1} = v_t$) satisfying: (1) each pair of adjacent vertices in \mathcal{P} has an edge $e(v_i, v_{i+1}) \in E$, (2) $\delta(\phi^{-1}(v_t), \phi^{-1}(v_{i+1})) < \delta(\phi^{-1}(v_t), \phi^{-1}(v_i))$, where $\phi^{-1}(v)$ denotes v 's vector $\vec{x}_v \in \mathcal{X}$ (Definition 2). This implies that the greater the number of hops (in a path) from v_i to v_t , the larger the distance between them in vector space. We call such a path from v_s to v_t a monotonic path $\mathcal{MP}(v_s, v_t)$.*

DEFINITION 7 (MONOTONIC SEARCH NETWORK). *Given a graph index $G(V, E)$ constructed for vector dataset \mathcal{X} . G is a Monotonic Search Network, iff $\forall v_s, v_t \in V, \exists \mathcal{MP}(v_s, v_t)$ on G .*

We provide a theorem showing the relation between the entry vertex selection and the upper bound on a routing path's length.

THEOREM 1. *Given a vector dataset \mathcal{X} distributed in a unit sphere \mathcal{B} in \mathbb{R}^d , a MSNET $G(V, E)$ constructed for \mathcal{X} , and a query vector $\vec{x}_q \in \mathcal{B}$. For query-sensitivity entry vertex selection strategy, we have N_{cluster} entry vertex candidates $\{v_{c_1}, \dots, v_{c_{N_{\text{cluster}}}}\}$, where v_{c_j} is the top-1 nearest neighbor to the centroid of cluster c_j . For the static graph-central entry vertex used in DiskANN, we use v_{c_0} to denote the entry vertex. Besides, we denote the top-1 nearest neighbor of \vec{x}_q within \mathcal{X} by \vec{x}_{q^*} and its corresponding vertex in G is $v_{q^*} = \phi(\vec{x}_{q^*})$. Given above*

assumptions, the following inequality holds for $j \in \{1, \dots, N_{\text{cluster}}\}$:

$$\overline{|\mathcal{MP}(v_{c_j}, v_{q^*})|} \leq \overline{|\mathcal{MP}(v_{c_0}, v_{q^*})|} \quad , \quad (2)$$

where $\overline{|\mathcal{MP}(\cdot, \cdot)|}$ represents the upper bound on the length of a Monotonic Path, i.e., the number of hops.

PROOF. We prove this theorem with the following two cases.

Case 1. Suppose we only have one cluster ($N_{\text{cluster}} = 1$), then we have $v_{c_1} = v_{c_0}$. This is because c_1 is the entire graph G and the central vertex of G actually is the top-1 nearest neighbor of the centroid of c_1 . Thus, we have $|\mathcal{MP}(v_{c_1}, v_{q^*})| = |\mathcal{MP}(v_{c_0}, v_{q^*})|$.

Case 2. For the case of $N_{\text{cluster}} > 1$, we introduce the concept of *open sphere* to derive the upper bound on a routing path's length.

Let $\mathcal{H}(\vec{x}_{q^*}, \theta)$ denotes an open sphere in \mathbb{R}^d with center \vec{x}_{q^*} and radius θ , $\mathcal{H}_{\text{vol}}(\vec{x}_{q^*}, \theta)$ denotes the volume of $\mathcal{H}(\vec{x}_{q^*}, \theta)$. Considering a monotonic path $\mathcal{MP}(v_{c_j}, v_{q^*})$ involving vertices $\{v_1, \dots, v_{l+1}, v_{q^*}\}$ ($v_1 = v_{c_j}$ is an entry vertex), for simplicity, we use the notation Vol_i to denote the volume of a sphere, i.e., $\text{Vol}_i = \mathcal{H}_{\text{vol}}(\vec{x}_{q^*}, \delta(\vec{x}_{q^*}, \vec{x}_{v_i}))$, for $i \in \{1, 2, \dots, l\}$. Since the volume of a sphere is calculated as

$$\mathcal{H}_{\text{vol}}(\cdot, \theta) = \frac{(\sqrt{\pi}\theta)^d}{\Gamma(\frac{d}{2} + 1)} \quad , \quad (3)$$

then we have the following for $i \in \{1, 2, \dots, l\}$:

$$\frac{\text{Vol}_{i+1}}{\text{Vol}_i} = \left(\frac{\delta(\vec{x}_{q^*}, \vec{x}_{v_{i+1}})}{\delta(\vec{x}_{q^*}, \vec{x}_{v_i})} \right)^d \quad . \quad (4)$$

We next show the relationship between terms $\delta(\vec{x}_{q^*}, \vec{x}_{v_{i+1}})$ and $\delta(\vec{x}_{q^*}, \vec{x}_{v_i})$. Given a cluster c_j , its diameter is $\bar{R} = \max_{\vec{x}_u, \vec{x}_v \in c_j} (\delta(\vec{x}_u, \vec{x}_v))$. We use $R^* = \min_{v_i, v_j \in \mathcal{MP}(v_s, v_{q^*}), v_s \in V, i \neq j} |\delta(\vec{x}_{q^*}, \vec{x}_{v_i}) - \delta(\vec{x}_{q^*}, \vec{x}_{v_j})|$ to represent the minimum distance difference in any monotonic path $\mathcal{MP}(v_s, v_{q^*})$ from an arbitrary vertex v_s to v_{q^*} . According to Definition 6, we have $\delta(\vec{x}_{q^*}, \vec{x}_{v_i}) > \delta(\vec{x}_{q^*}, \vec{x}_{v_{i+1}})$, so that $\delta(\vec{x}_{q^*}, \vec{x}_{v_i}) - \delta(\vec{x}_{q^*}, \vec{x}_{v_{i+1}}) \geq R^* > 0$ naturally holds. Thereby, due to $\bar{R} \geq \delta(\vec{x}_{q^*}, \vec{x}_{v_i}) \geq \delta(\vec{x}_{q^*}, \vec{x}_{v_{i+1}}) \geq \delta(\vec{x}_{q^*}, \vec{x}_{v_i}) - \delta(\vec{x}_{q^*}, \vec{x}_{v_{i+1}}) \geq R^*$, we have

$$\begin{aligned} \bar{R} \cdot (\delta(\vec{x}_{q^*}, \vec{x}_{v_i}) - \delta(\vec{x}_{q^*}, \vec{x}_{v_{i+1}})) &\geq \delta(\vec{x}_{q^*}, \vec{x}_{v_i}) \cdot R^* \\ \Rightarrow \frac{\bar{R} - R^*}{\bar{R}} &\geq \frac{\delta(\vec{x}_{q^*}, \vec{x}_{v_{i+1}})}{\delta(\vec{x}_{q^*}, \vec{x}_{v_i})} \quad . \end{aligned} \quad (5)$$

According to Eq. 4 and Eq. 5, we have

$$\frac{\text{Vol}_{i+1}}{\text{Vol}_i} \leq \left(\frac{\bar{R} - R^*}{\bar{R}} \right)^d \quad . \quad (6)$$

Next, we have the following derivation given $\overline{\text{Vol}} = \mathcal{H}_{\text{vol}}(\vec{x}_{q^*}, \bar{R})$:

$$\begin{aligned}
\text{Vol}_{l+1} &\leq \text{Vol}_l \cdot \left(\frac{\bar{R} - R^*}{\bar{R}}\right)^d \\
&\dots \\
&\leq \text{Vol}_1 \cdot \left(\frac{\bar{R} - R^*}{\bar{R}}\right)^{ld} \\
&\leq \overline{\text{Vol}} \cdot \left(\frac{\bar{R} - R^*}{\bar{R}}\right)^{ld} \\
\Rightarrow \log(\text{Vol}_{l+1}) &\leq \log(\overline{\text{Vol}}) + ld \cdot \log\left(\frac{\bar{R} - R^*}{\bar{R}}\right) \\
\Rightarrow l &\leq \frac{\log(\delta(\vec{x}_{q^*}, \vec{x}_{v_{l+1}})) - \log(\bar{R})}{\log(\bar{R} - R^*) - \log(\bar{R})} \\
&\triangleq f(\bar{R})
\end{aligned} \tag{7}$$

Above derivation shows the upper bound on the length of l is $f(\bar{R})$, we next analyze the monotonicity of $f(\bar{R})$ as

$$\begin{aligned}
\frac{df}{d\bar{R}} &= \frac{\frac{1}{\bar{R}}[\log \bar{R} - \log(\bar{R} - R^*)]}{(\log(\bar{R} - R^*) - \log(\bar{R}))^2} \\
&+ \frac{(\log \bar{R} - \log \delta(\vec{x}_{q^*}, \vec{x}_{v_{l+1}}))(\frac{1}{\bar{R} - R^*} - \frac{1}{\bar{R}})}{(\log(\bar{R} - R^*) - \log(\bar{R}))^2}
\end{aligned} \tag{8}$$

Since we have the following inequalities:

- $\log \bar{R} - \log(\bar{R} - R^*) > 0$,
- $\log \bar{R} - \log \delta(\vec{x}_{q^*}, \vec{x}_{v_{l+1}}) > 0$,
- $\frac{1}{\bar{R} - R^*} - \frac{1}{\bar{R}} > 0$,

the function $f(\bar{R})$ is monotonically increasing. Moreover, since we assume that $N_{\text{cluster}} > 1$, we have $\bar{R} \leq \frac{1}{2}$ and the following holds.

$$|\mathcal{MP}(v_{c_j}, v_{q^*})| = f(\bar{R}) + 1 \leq f(\frac{1}{2}) + 1 = |\mathcal{MP}(v_{c_0}, v_{q^*})| \tag{9}$$

□

3.3 Complexity Analysis

Complexity. The time complexity of offline candidates generation stems from the mini-batch-kmeans. It has a time complexity of $O(r \cdot N_{\text{batch}} \cdot N_{\text{cluster}} \cdot d)$ [41], where r is the number of clustering iterations, N_{batch} is the mini-batch size, N_{cluster} is the number of entry vertices, and d is the dimensionality of a vector (d dominates the cost of distance calculation). The time complexity of online entry vertex selection arises from the linear scanning of all candidates and their distance calculations. It has a time complexity of $O(N_{\text{cluster}} \cdot d)$.

Remarks. (1) The run-time efficiency improvement brought by query-sensitivity entry vertex comes from the trade-off between the time spent for online entry vertex selection and the time saved for SSD I/O due to the shortened routing path. Since reading a SSD page is much slower (at least 10 X slower) than that of reading from memory, it's natural to see that we have a good efficiency compared with the original DiskANN. (2) The time for online entry vertex selection is dominated by N_{cluster} given a specific d , so that setting an appropriate N_{cluster} is critical. Generally, we prefer a smaller N_{cluster} to decrease the overhead of online entry vertex selection, when SSD's I/O bandwidth is large (or we say that SSD I/O is fast).

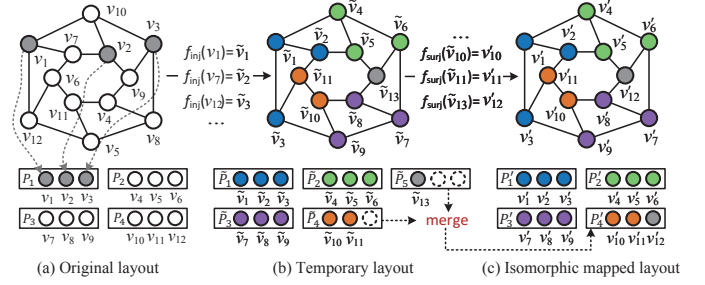


Figure 3: Isomorphic mapping on graph index

Otherwise, a larger N_{cluster} would be better. We experimentally show N_{cluster} 's effect under diverse SSD I/O bandwidth in §6.5.

4 ISOMORPHIC MAPPING ON VAMANA

The second I/O issue of DiskANN, i.e., the redundant I/O requests, is mainly caused by the low data value of each SSD page. Since each SSD page contains only a small amount of useful information for node expansion (Algorithm 1: lines 12-15), it increases the total number of I/O requests (Algorithm 1: line 11). As a result, many pages would be redundantly accessed. So, we present an isomorphic mapping on Vamana to refine its SSD layout, thus increasing the data value of each SSD page (§4.1), then analyze its effectiveness via *algebraic connectivity* [16] (§4.2), and show its complexity (§4.3).

4.1 Pack-Merge-based Method

Given the page capacity of b , DiskANN writes data blocks to SSD pages in a round-robin manner (Figure 3(a)). In this way, we can quickly compute a given vertex's resident page, yielding an efficient addressing on SSD. For example, given an arbitrary vertex v_i , we know that b_{v_i} is the $i\%b$ -th data block of the $\lceil \frac{i}{b} \rceil$ -th SSD page.

In this section, we aim to refine the SSD layout so that increase the data value of each SSD page, while keeping the original addressing mode unchanged. Achieving this is non-trivial. *Edge-based graph partitioning* methods [42, 56, 61] suffer from the redundancy in vertices, e.g., one vertex would appear multiple times in different SSD pages, invalidating the calculation of SSD offsets using vertex IDs. *Vertex-based graph partitioning* methods [35, 49, 50] fail to ensure that each SSD page contains the same number of vertices, also undermining the calculation of SSD offsets. *Graph reordering* method [54] keeps the addressing mode unchanged, their inevitable requirement to load the entire graph and construct a reverse index in memory render them inapplicable to large-scale graphs.

Different from them, we present a low-memory overhead, low-time complexity lightweight isomorphic mapping on Vamana, while retaining the original rapid SSD addressing mode.

DEFINITION 8 (ISOMORPHIC MAPPING). Given two SSD layouts L and L' for graphs $G = (V, E)$ and $G' = (V', E')$, respectively. We say $f: L.\text{IDs} \rightarrow L'.\text{IDs}$ is an isomorphic mapping on their logical view (or logical layout), iff f is a bijection satisfying three conditions: (1) L and L' contain the same number of data blocks. (2) $\forall b_{v_i}, b_{v_j} \in L$, if their identities $v_i \neq v_j$, then $f(v_i) \neq f(v_j)$. (3) $\forall b_{v_i}, b_{v_j} \in L$, if $\exists e(v_i, v_j) \in E$, then $e(v'_i, v'_j) \in E'$ where $v'_i = f(v_i)$ and $v'_j = f(v_j)$.

Figure 3(c) shows an isomorphic mapped SSD layout of a graph. Each data block b_v of a vertex $v \in V$ has a mapped $b'_{v'}$ of a vertex

Algorithm 3: Packing($G, L.\text{IDs}, b$)

Input: graph index G , logical layout $L.\text{IDs}$, page capacity b
Output: temporary logical layout $\tilde{L}.\text{IDs}$ with an injection f_{inj}

// Initialization: line 1

- 1 Visit $\leftarrow \emptyset$, $\tilde{L}.\text{IDs} \leftarrow \emptyset$, newID $\leftarrow 1$, $f_{\text{inj}} \leftarrow \emptyset$
 // Star packing: lines 2-18
- 2 **for** $v \in V \& v \notin \text{Visit}$ **do**
- 3 Visit $\leftarrow \text{Visit} \cup \{v\}$;
- 4 $\tilde{P}.\text{IDs} \leftarrow \{v\}$; /* create a temporary logical page */
- 5 sort $N(v) \subseteq V$ in ascending order of PQ distance; /* update $\tilde{P}.\text{IDs}$ with at most b vertices */
- 6 **for** $v_i \in N(v)$ in order **do**
- 7 **if** $|\tilde{P}.\text{IDs}| < b$ **then**
- 8 $\tilde{P}.\text{IDs} \leftarrow \tilde{P}.\text{IDs} \cup \{v_i\}$;
- 9 Visit $\leftarrow \text{Visit} \cup \{v_i\}$;
- 10 **else**
- 11 | break ;
- 12 **end**
- 13 **end**
- 14 **if** $|\tilde{P}.\text{IDs}| < b$ **then**
- 15 | pad $\tilde{P}.\text{IDs}$ with zero; /* logical page alignment */
- 16 **end**
- 17 $\tilde{L}.\text{IDs} \leftarrow \tilde{L}.\text{IDs} \cup \tilde{P}.\text{IDs}$
- 18 **end**
- // Injection from $L.\text{IDs} \rightarrow \tilde{L}.\text{IDs}$: lines 19-26
- 19 **for** $\tilde{P}.\text{IDs} \subset \tilde{L}.\text{IDs}$ **do**
- 20 **for** $v_i \in \tilde{P}.\text{IDs}$ **do**
- 21 $j = \text{newID}++$;
- 22 $f_{\text{inj}}.\text{put}(v_i, \tilde{v}_j)$; /* update f_{inj} with $f_{\text{inj}}(v_i) = \tilde{v}_j$ */
- 23 update $\tilde{P}.\text{IDs}$ with \tilde{v}_j ;
- 24 **end**
- 25 $\text{newID} = (\lceil \frac{\text{newID}}{b} \rceil - 1) \cdot b + 1$;
- 26 **end**
- 27 **return** $\tilde{L}.\text{IDs}$ and f_{inj} ;

$v' \in V'$ and all the data blocks on SSD pages retain the ascending order of vertex ID, thus we can efficiently access SSD pages using the same addressing mode as DiskANN. Since there exists various isomorphic mapping f , we need to implement one that can increase the data value of SSD pages. So, we present our *pack-merge-based method* to return a logical layout $L'.$ IDs with an isomorphic mapping $f : L.\text{IDs} \rightarrow L'.$ IDs. It consists of two steps: packing (Algorithm 3) and merging (Algorithm 4). Packing aims to return a temporary logical layout $\tilde{L}.\text{IDs}$ by an injection f_{inj} from $L.\text{IDs}$ (see Figure 3(b)) and merging aims to return a final logical layout $L'.$ IDs by a surjection f_{surj} from $\tilde{L}.\text{IDs}$. In this way, the isomorphic mapping $f = f_{\text{surj}}(f_{\text{inj}}(\cdot))$ is a bijection from $L.\text{IDs}$ to $L'.$ IDs.

Packing stage. Given an SSD-resident graph index $G = (V, E)$ and a page capacity b , the packing algorithm (Algorithm 3) returns a temporary logical layout $\tilde{L}.\text{IDs}$ with f_{inj} by three steps.

Initialization. We initialize a set $\text{Visit} = \emptyset$ to avoid repeated vertex visits, a temporary logical layout $\tilde{L}.\text{IDs} = \emptyset$, a vertex ID iterator newID starting from 1, and an empty map f_{inj} (line 1).

Star packing. We generate $\tilde{L}.\text{IDs}$ as follows. For each unvisited vertex $v \in V$, we add it to a temporary logical page $\tilde{P}.\text{IDs}$ and mark it as a visited vertex (lines 3-4). Then, we add v 's $(b - 1)$ nearest neighbors (using PQ distance) from G to the same logic page $\tilde{P}.\text{IDs}$ (lines 5-13). If $N(v) < b$, we pad $\tilde{P}.\text{IDs}$ with zeros (lines 14-16). We next add $\tilde{P}.\text{IDs}$ to $\tilde{L}.\text{IDs}$ and repeat above (line 17) until all vertices of V have

Algorithm 4: Merging($\tilde{L}.\text{IDs}, b$)

Input: temporary logical layout $\tilde{L}.\text{IDs}$, page capacity b
Output: final logical layout $L'.$ IDs with an surjection f_{surj}

// Initialization: lines 1-2

- 1 $L' \leftarrow \emptyset$, newID $\leftarrow 1$, $f_{\text{surj}} \leftarrow \emptyset$
- 2 sort temporary logical pages of $\tilde{L}.\text{IDs}$ in descending order of page size, i.e., the number of non-zero logical blocks;
- 3 **for** $\forall \tilde{P}_i.\text{IDs} \subset \tilde{L}.\text{IDs}$ in order **do**
- 4 **if** $|\tilde{P}_i.\text{IDs}| == b$ **then**
- 5 $P'_i.\text{IDs} \leftarrow \tilde{P}_i.\text{IDs}$; /* copy as a new logical page */
- 6 $\tilde{L}.\text{IDs} \leftarrow \tilde{L}.\text{IDs} \setminus \tilde{P}_i.\text{IDs}$;
- 7 **else**
- 8 // FFD-based merge: lines 8-13
- 9 **for** $\forall \tilde{P}_j.\text{IDs} \in \tilde{L}.\text{IDs}$ in order **do**
- 10 **if** $|\tilde{P}_i.\text{IDs}| + |\tilde{P}_j.\text{IDs}| \leq b$ **then**
- 11 $P'_i.\text{IDs} \leftarrow \tilde{P}_i.\text{IDs} + \tilde{P}_j.\text{IDs}$; /* merge */
- 12 $\tilde{L}.\text{IDs} \leftarrow \tilde{L}.\text{IDs} \setminus \tilde{P}_i.\text{IDs} \cup \tilde{P}_j.\text{IDs}$;
- 13 **end**
- 14 **end**
- 15 // Surjection from $\tilde{L}.\text{IDs} \rightarrow L'.$ IDs: lines 15-21
- 16 **for** $\forall \tilde{v}_i \in P'_i.\text{IDs}$ **do**
- 17 $j = \text{newID}++$;
- 18 $f_{\text{surj}}.\text{put}(\tilde{v}_i, v'_j)$; /* update f_{surj} with $f_{\text{inj}}(\tilde{v}_i) = v'_j$ */
- 19 update $P'_i.\text{IDs}$ with v'_j ;
- 20 **end**
- 21 $\text{newID} = (\lceil \frac{\text{newID}}{b} \rceil - 1) \cdot b + 1$;
- 22 $L'.$ IDs $\leftarrow L'.$ IDs $\cup P'_i.\text{IDs}$;
- 23 **end**
- 24 **return** $L'.$ IDs and f_{surj} ;

been visited. Since v and its top- $(b - 1)$ nearest neighbors belong to the same page, the induced graph of them is a star-derived graph. In §4.2, we provide an effectiveness analysis of our pack-merge-based method using the properties of star-derived graph.

Injective mapping. Given a temporary logical layout $\tilde{L}.\text{IDs}$, we obtain the injection f_{inj} as follows. First, for each vertex $v_i \in \tilde{P}.\text{IDs} \subset \tilde{L}.\text{IDs}$, we update f_{inj} with an item $f(v_i) = \tilde{v}_j$, where $j = \text{newID}$ (lines 20-24). We next update newID (line 25) and repeat above until all logical pages in $\tilde{L}.\text{IDs}$ have been visited.

EXAMPLE 1. Figure 3(b) shows a temporary logical layout after packing the layout in Figure 3(a). We use the same color to represent the vertices in the same temporary page. Given the page capacity $b = 3$, we first assign v_1 and its two nearest neighbors v_7, v_{12} to the first page, pad non-full pages with zeros (e.g., the fourth and fifth pages), and repeat this until all vertices are processed (Algorithm 3: lines 2-18). Next, we update the vertex IDs and record the injection f_{inj} with the mapping from original vertex IDs to the new temporary vertex IDs, e.g., $f_{\text{inj}}(v_1) = \tilde{v}_1, f_{\text{inj}}(v_2) = \tilde{v}_5, f_{\text{inj}}(v_3) = \tilde{v}_6$, etc.

Merging stage. The temporary logical layout still has one problem: some pages are not full (as we pad zeros for nodes having neighbors $< b$), and it invalids the original addressing mode. So, we present a merging stage with the goal of implementing a surjection $f_{\text{surj}} : \tilde{L}.\text{IDs} \rightarrow L'.$ IDs to combine data blocks from non-full pages to form a new full page. Given a temporary logical layout $\tilde{L}.\text{IDs}$ and a page capacity b , we do merging (Algorithm 4) as follows.

Initialization. We initialize a final logical layout $L'.$ IDs $\leftarrow \emptyset$, a vertex ID iterator newID starting from 1, and an empty map f_{surj} (line 1).

FFD-based merge. We generate $L'.IDs$ as follows. We first sort temporary logical pages of $\tilde{L}.IDs$ in descending order of page size. The logical page's size is the number of non-zero logical blocks in it, denoted by $|\tilde{P}.IDs|$. We retain the temporary logical pages with size $= b$ in $L'.IDs$ (lines: 4–6 and 21) and merge others having size $< b$ to form new logical pages (lines: 8–13 and 21). Specifically, we merge two temporary logical pages by bin packing based on First-Fit-Decreasing (FFD): we iteratively merge the largest non-full logical page with another smaller logical page to form a new full logical page until no more merge can be performed.

Surjection mapping. Given a new logical page $P'.IDs$ that is retained from $\tilde{P}.IDs$ (line 5) or merged by two logical pages from $\tilde{L}.IDs$ (line 10), we obtain the surjection f_{surj} as follows. First, for every vertex \tilde{v} from $P'.IDs$, we update f_{surj} with an item $f_{\text{surj}}(\tilde{v}_i) = v'_j$, where $j = \text{newID}$ (lines 15–19). Next, we update newID (line 20) and add $P'.IDs$ to the logical layout $L'.IDs$ (line 21). We repeat above until all logical pages from $\tilde{L}.IDs$ have been processed and return the final logical layout $L'.IDs$ with the surjection f_{surj} (line 23).

EXAMPLE 2. Figure 3(c) shows the final layout after merging the layout in Figure 3(b). Since the first three are full pages, they are retained in the final logical layout. For the fourth page, it contains only two valid vertices so that we merge it with the last page. Then, we update the vertex IDs and record the surjection f_{surj} with the mapping from the temporary vertex IDs to the final vertex IDs, e.g., $f_{\text{surj}}(\tilde{v}_{10}) = v'_{10}$, $f_{\text{surj}}(\tilde{v}_{11}) = v'_{12}$, and $f_{\text{surj}}(\tilde{v}_{13}) = v'_{12}$.

Update the SSD layout using f_{inj} and f_{surj} . Given the original logical layout $L.IDs$ and the output final logical layout $L'.IDs$ with two mappings f_{inj} and f_{surj} , we update SSD layout L' with the real data blocks as follows. Given a logical page $P.IDs \subset L.IDs$, for each vertex $v_i \in P.IDs$ with data block $b_{v_i} = \langle \vec{x}_i, N(v_i) \rangle$, we first get v_i 's mapping vertex $v'_j = f_{\text{surj}}(f_{\text{inj}}(v_i))$. Then, we form $b_{v'_j}$ as $\langle \vec{x}_{v'_j}, N(v'_j) \rangle$, where $\vec{x}_{v'_j} = \vec{x}_{v_i}$ because both v_i and v'_j represent the same vertex but with different IDs. For each vertex from $N(v_i)$, we obtain its mapping vertex using $f_{\text{surj}}(f_{\text{inj}}(\cdot))$ and add it to $N(v'_j)$. Finally, we write all reformed data blocks to their correspond positions in L' according to the final logical layout $L'.IDs$.

4.2 Effectiveness Analysis of Refined Layout

Since our intention is to increase the data value of each SSD page, it is necessary to evaluate the compactness of a SSD page after isomorphic mapping. We present a new metric called *page compactness* based on two widely used metrics: *diameter* and *algebraic connectivity* [16] of a graph. Graph diameter is defined as the longest shortest path between any two vertices of a graph. The larger the diameter, the less the closeness between any two vertices. Given a SSD page consisting of b data blocks, we compute the diameter of the induced graph $G[V_b]$ of these b vertices by Eq. 10, where $\text{shortest_path}(u, v)$ returns the length of the shortest path between vertices u and v .

$$\text{diam}(G[V_b]) = \max_{u, v \in V_b} \text{shortest_path}(u, v) \quad (10)$$

Table 1: Page compactness of two SSD layouts (original and isomorphic) for Vamana built on different datasets.

SSD layout ↓	sift100M (R32)	deep100M (R32)	turing100M (R32)
original layout	0.000004	0	0
isomorphic mapped layout	0.658033	0.560141	0.547292

Algebraic connectivity is another metric that reflects the global connectivity among vertices in a graph. It is defined as the second-smallest eigenvalue of the Laplacian matrix [16] of a graph. Given a induced graph $G[V_b]$ of a SSD page's b vertices, its algebraic connectivity $\lambda_2(G[V_b])$ is computed by Eq. 11, where $\text{Lap}(G[V_b])$ is the Laplacian matrix of $G[V_b]$ and ξ is the eigenvector of $\text{Lap}(G[V_b])$.

$$\lambda_2(G[V_b]) = \min_{\substack{\xi \perp 1 \\ \xi \neq 0}} \frac{\xi^T \text{Lap}(G[V_b]) \xi}{\xi^T \xi} \quad (11)$$

Given a graph $G[V_b]$, its Laplacian matrix is computed as

$$\text{Lap}_{(i,j)}(G[V_b]) = \begin{cases} \deg(v_i) & \text{if } i = j \\ -1 & \text{if } i \neq j \text{ and } v_i \text{ is adjacent to } v_j \\ 0 & \text{otherwise} \end{cases} \quad (12)$$

Given above two metrics, we define the page compactness as

$$\gamma(G[V_b]) = \frac{\lambda_2(G[V_b])}{\text{diam}(G[V_b])} \quad (13)$$

Note that, the smaller (larger) the diameter (algebraic connectivity), the greater the page compactness. Table 1 provides the page compactness of the original SSD layout and isomorphic mapped SSD layout of the Vamana built on three datasets using the same parameter $R = 32$. In DiskANN, R is the largest out-degree of Vamana that is used to control the index construction. Since DiskANN assigns data blocks on SSD in a round-robin manner, vertices in a SSD page are almost disconnected in Vamana. As a result, many SSD pages' algebraic connectivity is close to zero, resulting in a high probability that the page compactness tends to zero. For ours, given a vertex v , we assign its $b - 1$ neighbors to the same page of v (Algorithm 3: lines 6–13). Hence, the induced graph of them is a typical star-derived graph. Given this premise, we prove that the page compactness of ours must > 0.5 in Theorem 2.

DEFINITION 9 (STAR-DERIVED GRAPH). Given a graph $G = (V, E)$ with one central vertex $v \in V$ and other $|V| - 1$ peripheral vertices $V \setminus v$. We call G a star graph if all peripheral vertices have edges to v but no edges among peripheral vertices. Given another graph $G' = (V, E')$ that have the same vertices as G and $E' \supset E$, then we call G' a star-derived graph, i.e., derived from the star graph G .

THEOREM 2. Given a SSD page of the isomorphic mapped layout of Vamana, its page compactness must > 0.5 .

PROOF. In a star graph, its diameter is fixed to 2 and its algebraic connectivity is constantly at 1. Since a star-derived graph allows connections among peripheral vertices, it may decrease the diameter (or we say it has a diameter $\text{diam}(\cdot) \leq 2$) and it would certainly increase the algebraic connectivity (i.e., $\lambda_2(\cdot) > 1$). As a result, the page compactness of isomorphic mapped layout must > 0.5 . \square

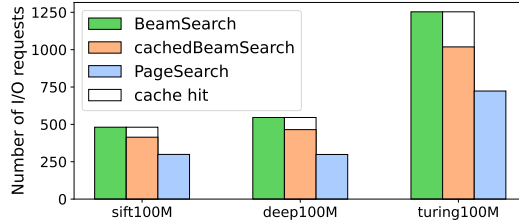


Figure 4: The number of I/O requests (SSD and cache I/O) of beamsearch, cachedBeamsearch, and pagesearch.

4.3 Complexity Analysis

Time Complexity. The complexity arises from both packing and merging. Assuming that basic arithmetic operations can be performed in $O(1)$ time, the complexity of packing is $O(|V| \cdot R \cdot d)$, where $|V|$ is the total number of vertices in a graph G , R is the largest out-degree, and d is the dimensions. This is because we need to calculate the PQ distances between each vertex $v \in V$ and its all R neighbors and select the nearest $b - 1$ neighbors as well as v to form a SSD page. The complexity of merging is evidently $O(b \cdot N)$. So, the overall time complexity of the mapping is $O(|V| \cdot R \cdot d + b \cdot N)$.

Space Complexity. We analyze the space complexity related to memory usage here. Packing requires the computation of PQ distances between vectors, and we also need to maintain the mapping f_{inj} . If we consider the space complexity of storing a basic data type as $O(1)$, then the space complexity of packing is $O(|V| + |V| \cdot d)$, while merging does not incur any additional space complexity.

5 PAGE-BASED SEARCH

In this section, we discuss how to use the refined SSD layout of isomorphic mapped Vamana to accelerate the beamsearch. A straightforward idea is to cache all the read SSD pages and check the cache before requesting subsequent SSD pages to avoid redundant SSD I/O requests. It's worth mentioning that this method would not reduce the total number of I/O requests but only replace a part of heavyweight SSD I/O requests with efficient cache I/O requests. The greater the cache hit rate is, the larger the QPS can be achieved. We have implemented this simple method called cachedBeamsearch and compare it with the original beamsearch. Figure 4 shows that cachedBeamsearch (middle bar) has the same number of I/O requests as beamsearch (left bar), of which only 10%-20% I/O requests are hit in cache and most of the cached SSD pages are remained unused for the node expansion step of beamsearch. Moreover, the CPU remained largely underutilized during the search process due to the passive nature of cache requests. In order to take the advantages of refined SSD layout, we propose an active filtering-based asynchronous page expansion as a complement to node expansion, thus forming a new pagesearch as an alternative to beamsearch.

Figure 5 illustrates the pipelines of our pagesearch and beamsearch. Pagesearch relies on a meticulously customized page cache pool called page heap (discussed in §5.1). It involves four basic operators: `Cache()`, `Update()`, `Check2ret()`, and `Pop()` (the green components in Figure 5(b)), based on which we design a page expansion strategy to actively filter more useful vertices as candidates for node expansion. Besides, we leverage the CPU's stall cycle (shown in Figure 5(a)) to perform the proposed page expansion asynchronously,

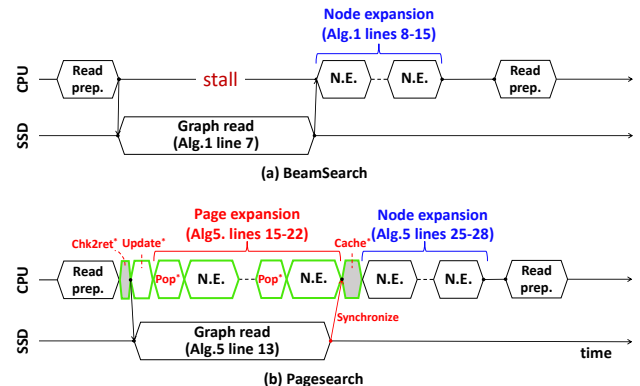


Figure 5: Pipeline of original Beamsearch and our Pagesearch (N.E. refers to NeighborExpansion).

when the SSD I/O requests are processing at the same time. In this way, we improve the CPU utilization so as to improve overall QPS. Figure 4 shows that pagesearch (right bar) achieves nearly 50% reduction of SSD I/O requests compared with beamsearch.

5.1 Page Heap

PageHeap is a page cache pool with the following basic operators.

- (1) `Cache()`. It caches a 4k-aligned page into the memory pool and register the vertices within the page into a circular queue.
- (2) `Update()`. It first calculates the full vector distance between each vertex in the circular queue and a query. Based on these distances, it updates a min-heap using these vertices and remove them from circular queue. This min-heap would be used in the page expansion step (we discuss it in §5.2).
- (3) `Check2ret()`. It checks whether a given page's data block exists in the memory pool. If the data block is found, it is returned as the output, otherwise it reports none.
- (4) `Pop()`. It popups the top-1 vertex having the minimum distance to the given query, from the min-heap.

5.2 Pagesearch

Given a SSD-resident graph index $G = (V, E)$ of the vector dataset X , query vector \vec{x}_q , beam size B , search width L_s , and the desired k of top- k , Algorithm 5 shows the procedure of pagesearch in detail.

Initialization. We initialize the candidate set C as the entry vertex $\{v_e\}$, the top- k results $\mathcal{R} = \emptyset$, and the page heap $\mathcal{H} = \emptyset$ (lines 1-3).

Read Preparing. We prepare SSD I/O requests for the unvisited top- B vertices from C , denoted by \mathcal{F} . For each $v_i \in \mathcal{F}$, we invoke `check2ret()` to check if v_i is cached and create page placeholders P_j into \mathcal{P} to register read requests for uncached vertices (lines 6-12). We submit the prepared read requests asynchronously (line 13).

Page Expansion. While asynchronously handling read requests, we invoke `Update()` to update page heap (line 14) and begin page expansion. We iteratively `Pop()` one vertex from page heap and invoke `NeighborExpansion` (Algorithm 2) to update both C and \mathcal{R} with more promising candidates (lines 15-22). We terminate this page expansion when asynchronous SSD read completes (lines 18-20) in order to make it synchronized with the asynchronous read.

Algorithm 5: Pagesearch($G, \vec{x}_q, v_e, B, L_s, k$)

Input: graph index G , query \vec{x}_q , enterpoint v_e , beam size B , search width L_s , size k of top- k

Output: approximate nearest top- k neighbors \mathcal{R} to \vec{x}_q

```

1  $C \leftarrow \{v_e\}$ ; /* candidate set initialized as  $\{v_e\}$  */
2  $\mathcal{R} \leftarrow \emptyset$ ; /* top- $k$  results initialized as empty */
3  $\mathcal{H} \leftarrow \text{PageHeap}()$ ; /* PageHeap initialized as empty */
4 do
5    $\mathcal{F} \leftarrow \text{top-}B \text{ unvisited vertices from } C \text{ for expansion}$  ;
  // prepare for SSD I/O requests: lines 6-12
6    $\mathcal{P} \leftarrow \emptyset$ ; /* page placeholders initialized as empty */
7   for  $v_i \in \mathcal{F}$  do
8     if  $\mathcal{H}.\text{check2ret}(v_i)$  is none then
9        $P_j \leftarrow \text{register read for page containing } b_{v_i}$  ;
10       $\mathcal{P} \leftarrow \mathcal{P} \cup P_j$  ;
11    end
12  end
13  // async SSD I/O requests: line 13
14  async read all pages in  $\mathcal{P}$  from SSD ;
15   $\mathcal{H}.\text{update}()$  ;
16  // async page expansion: lines 15-22
17  while  $b_{v_i} = \langle \vec{x}_{v_i}, N(v_i) \rangle \leftarrow \mathcal{H}.\text{pop}()$  is not none do
18    if  $v_i$  is unvisited then
19      NeighborExpansion( $\vec{x}_q, b_{v_i}, C, \mathcal{R}, L_s, k$ ) ;
20      if async read done then
21        | break ;
22      end
23    end
24    wait for async read done ;
25     $\mathcal{H}.\text{cache}(\mathcal{P})$  ;
26    // node expansion: lines 25-28
27    for unvisited  $v_i \in \mathcal{F}$  do
28       $b_{v_i} = \langle \vec{x}_{v_i}, N(v_i) \rangle \leftarrow \mathcal{H}.\text{check2ret}(v_i)$  ;
      NeighborExpansion( $\vec{x}_q, b_{v_i}, C, \mathcal{R}, L_s, k$ ) ;
29    end
30  return  $\mathcal{R}$ 
31 while  $\mathcal{F} \neq \emptyset$ ;
```

Table 2: Statistics of datasets

Dataset	Dimension	LID [15]	Query	Base (M:10 ⁶ , B:10 ⁹)
image ¹	100	15.3	10,000	100M
sift [2]	128	16.6	10,000	100M
deep [60]	96	17.6	10,000	10M~1B
msong [3]	420	18.0	200	0.99M
crawl [4]	300	27.4	10,000	1.99M
turing [62]	100	30.5	100,000	100M
glove-100 [30]	100	34.3	10,000	1.18M
gist [2]	960	35.0	1,000	1M

Node Expansion. When page expansion finishes, we execute the same node expansion process as beamsearch: taking unvisited node's data block b_{v_i} from the memory pool of page heap by invoking `check2ret()`, for further NeighborExpansion. Pagesearch repeats the read preparing, page expansion, and node expansion until no more vertex is visited and returns the top- k results \mathcal{R} .

6 EVALUATION

We present a detailed comparative analysis between our DiskANN++, DiskANN, and other competitors, to answer four key questions:

Q1: Does DiskANN++ achieve a better balance between QPS and recall@100 than others within a low memory footprint (**§6.2**)?

Q2: Does DiskANN++ consistently outperform DiskANN under various hardware resource constraints (**§6.3**)?

Q3: How's the scalability of our DiskANN++ w.r.t. different datasets (with various hardness measured by LID) and data scales (**§6.4**)?

Q4: What is the parameter sensitivity for DiskANN++ (**§6.5**)?

6.1 Experiment Settings

Datasets. Our experiments encompass a total of eight datasets, including seven publicly available datasets (msong [3], glove-100 [30], crawl [4], gist [2], sift [2], deep [60], and turing [62]) and one commercial dataset (image¹). The slices of deep ranging in size from 1M to 1B were employed for evaluating the stability w.r.t. data scales. Detailed statistics of these datasets are provided in Table 3.

Comparing algorithms. We implemented our DiskANN++ and compared it with three SSD-based solutions: (1) SPANN [11]. It uses vertices on a spatial partition tree to represent clusters of the dataset and conducts search based on inverted indexing. (2) BBANN [47]. It uses vertices of a nearest neighbor graph to represent clusters of the dataset aligned in disk blocks and conducts a nearest neighbor search to determine the clusters containing nearest neighbors for filtering. (3) DiskANN [29]. It is a PQ-based hybrid method that aims to reduce memory usage while ensuring a high search accuracy.

Resource Constraints. We conducted experiments under varying hardware conditions via Docker technology, including memory constraints from 2GB to 10GB, 1 to 8 different threads, and different 4k random I/O bandwidth ranging from 100MB/s to 700MB/s.

Evaluation Metrics. We evaluate ANNS's effectiveness by *recall@100*. We evaluate ANNS's efficiency by *QPS* and *speedup*. Speedup is defined as the ratio of QPS achieved by DiskANN++ and DiskANN when both algorithms attain the same recall@100.

Implementation Setup. For SPANN, BBANN, and DiskANN, we use public implementations provided in their respective GitHub repositories. All algorithms were compiled in C++17, retaining relevant SIMD and prefetching instructions. The benchmark scripts were implemented using Bash and Python3. And all experiments were conducted on an Ubuntu 20.04 server platform with the following hardware configuration: CPU-Intel Core i9-10900X (3.70GHz), SSD-PM981 2TB, DRAM-32GB, and 2133Mb/s DDR4 x4.

6.2 Effectiveness and Efficiency Evaluation

In this test, all searches were conducted using 8 threads with fully utilized I/O resources. The QPS vs. recall@100 result and memory usage vs. recall@100 are presented in Figure 6. We ensured that DiskANN and DiskANN++ utilized the same low amount of memory (10% of the dataset size). For SPANN and BBANN, since they required at least 20% of the dataset size in memory to gain an acceptable recall (>85%) using the parameters recommended in original papers, we set the memory constraint for them as 20%.

Balance of QPS and recall@100. Our evaluations demonstrate that the DiskANN family of algorithms strikes a better balance between QPS and recall than that of SPANN and BBANN at high recall. DiskANN++ achieves a 50%-100% improvement over DiskANN under the same recall@100. For example, given the same recall@100 as 97% in deep100M, the QPS of DiskANN++ and DiskANN are

¹Commercial image dataset provided by Huawei Technologies Co., Ltd, China

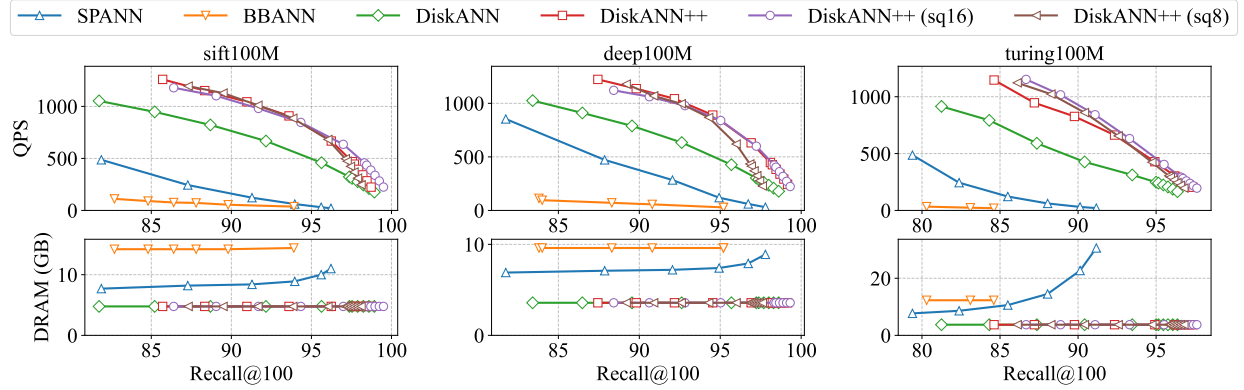


Figure 6: QPS and DRAM usage vs. Recall@100 for SPANN, BBANN, DiskANN, and DiskANN++ (with sq16/sq8 compression)

605.3 and 310.2, respectively, resulting a significantly 95% improvement on QPS. In scenarios where node compression is used, we run all algorithms under different compression ratio such as sq16 and sq8. Here, sq16 means that we compress the vector data in each node from fp32 to int16. The larger the number, the smaller the compression ratio, and the less the precision loss of original vector. For the case of using sq16, it shows the similar trends as that without compression. Besides, the sq16 compression slightly improves the QPS given the same recall@100. This is because it reduces the word length of node data by compressing vector with less precision loss, which allows for accommodating more nodes in each SSD page. Consequently, it increases the page expansion width (i.e., *b*) in Pagesearch, which, to a certain extent, accelerates the convergence speed of the search process. On the other hand, we found that a noticeable drop occurs at high recall when we used sq8 compression. This is because the significant precision loss of original vector when a strong compression is conducted.

Memory Usage. As shown in Figure 6, SPANN and BBANN consume significantly more memory than DiskANN family of algorithms and the memory usage continues to grow as the precision increases. The reason is two-folded: (1) SPANN and BBANN inevitably require reading more disk clusters to achieve higher precision, resulting in ever-increasing memory consumption, and (2) SPANN and BBANN still maintain graph index in memory, which inherently demand more memory resources. In contrast, the DiskANN family of algorithms maintains a stable memory footprint that remains substantially lower than the former because of the PQ technique used to obtain low-dimensional quantized vectors resident in memory.

6.3 Effect of Hardware Resources

We conducted experiments on deep100M, sift100M, and turing100M, under varying I/O bandwidth (Figure 7(a)), # threads (Figure 7(b)), and DRAM usage constraints (Figure 7(c)), to show the effect of hardware resources on speedup given the high recall@100 of 97%.

Effect of # threads and I/O limits. In Figure 7(a)-(b), it is evident that DiskANN++ achieves consistent speedup across varying # threads and I/O limits on the same dataset. The differences of speedup across datasets can be attributed to the impact of dataset's dimensions and the influence of varying local intrinsic dimensionality (LID) on search lengths, as discussed in [36].

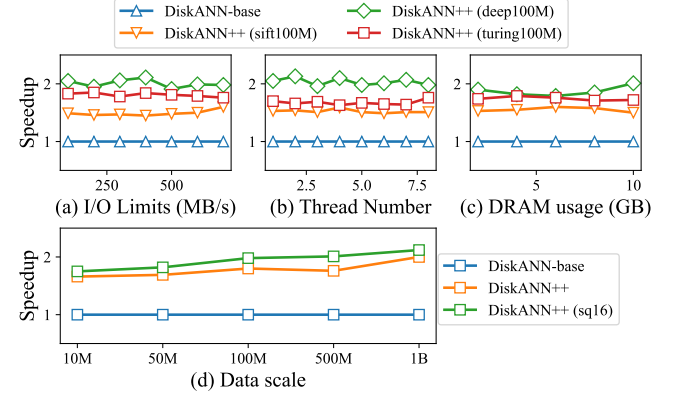


Figure 7: Speedup of DiskANN++ compared to DiskANN under different (a) I/O bandwidth, (b) thread number, (c) DRAM usage constraint, and (d) dataset scale (deep: 10M~1B).

Table 3: QPS and speedup results of different datasets

Datasets↓		DiskANN	DiskANN++	DiskANN++ (sq16)		
dataset	LID	QPS	QPS	speedup	QPS	speedup
image	15.3	77.53	117.07	1.51x	143.57	1.85x
sift100M	16.6	354.1	523.32	1.48x	599.18	1.69x
deep100M	17.6	310.24	605.31	1.95x	617.77	1.99x
msong	18.0	435.99	653.35	1.50x	829.48	1.90x
crawl	27.4	738.2	1209.03	1.64x	1318.63	1.79x
turing100M	30.5	110.70	270.65	2.44x	289.77	2.61x
glove-100	34.3	90.66	245.49	2.71x	278.83	3.08x
gist	35.0	348.32	347.7	1.00x	474.93	1.36x

Effect of DRAM usage constraints. In the DiskANN framework, the primary impact of memory constraints is on the compression rate of the PQ in memory, i.e., the precision loss of original vector. A lower memory usage constraint leads to a higher compression rate of PQ, resulting a larger precision loss of original vector. Since we fix the recall@100 as 97% to collect the experiment results, the effect of memory constraint is eliminated. This is why we still obtain a stable speedup even for a strict memory constraint (< 5GB).

6.4 Scalability Evaluation

In this subsection, we evaluated the scalability of DiskANN++ across different data scales (Figure 7(d)) and types of datasets (Table 4) given recall@100 of 97%. In Figure 7(d), the speedup is stable as the data scale increases. It is attributed to the adaptability of the graph index to various data scales. Some classical studies [19, 38]

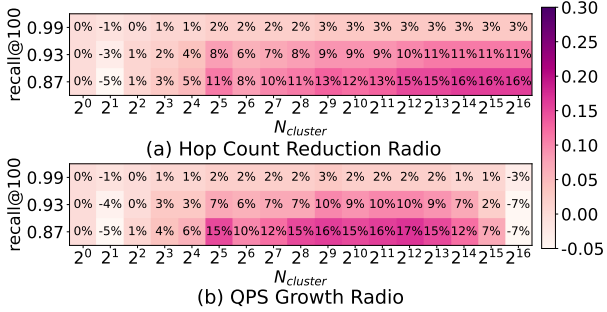


Figure 8: Effect of the query-sensitive entry vertex (with different N_{cluster}) under different recall@100 (deep100M).

have indicated that the time complexity of graph search is logarithmic which grows slowly with the increase of data scale. From Table 4, we found that ours achieves at least 1.5x speedup on most of the datasets except gist, due to its high vector dimensionality of 960, which results in only one vertex per page, limiting the effectiveness of pagesearch. However, after augmenting the node capacity to 2 with node compression of sq16, we achieved 1.36x improvement. We also noticed that our DiskANN++ is scalable to the hardness of datasets. For example, for truing100M and glove-100 datasets that have a LID > 30 (with a modest dimensionality of 100), we achieve at least 2.44x speedup. This is because when searching on the dataset with a larger LID, the NN refine phase constitutes a larger proportion and our pagesearch can effectively reduce the I/O requests in this phase (see Figure 2(d)), resulting in a good speedup.

6.5 Parameter Sensitivity

Effect of N_{cluster} . The cluster size N_{cluster} has a significant impact on query-sensitive entry vertex selection strategy. So, we study its influence in Figure 8. We found that increasing N_{cluster} can effectively reduce routing hops and improve the QPS, which aligns with the conclusion in Theorem 1 (§3.2). However, the search performance does not infinitely improve as N_{cluster} increases. This is because the time spent in entry vertex selection cannot be ignored. For example, using an excessively large $N_{\text{cluster}} = 2^{16}$ would increase the time on entry vertex selection, leading to a bad search performance. Therefore, it is necessary to carefully adjust N_{cluster} to achieve a favorable trade-off. Furthermore, as search precision (recall@100) increases, the QPS improvement brought by query-sensitive entry vertex selection strategy diminishes. This is because the routing procedure requires more time in NN refine step than NN approaching step to find the top- k with a high recall, thus weakening the improvement brought by query-sensitive entry vertex selection. We also study the effect of N_{cluster} on speedup under different I/O bandwidth (Table 4). It demonstrates that a smaller N_{cluster} is preferred to decrease the overhead of online entry vertex selection, when SSD’s I/O bandwidth is large (or we say that SSD I/O is fast). Otherwise, a larger N_{cluster} would be better.

Effect of beam size B . We study the effect of beam size B on speedup in deep100M. In Figure 9, speedup decreases as the beam size increases. This is because increasing the beam size explicitly expands the width of node expansion, allowing node expansion to process more data blocks from page heap in each iteration, resulting

Table 4: Effect of N_{cluster} on speedup under different I/O bandwidth (varied from 100 MB/s to 700 MB/s).

$N_{\text{cluster}} \downarrow$	I/O bandwidth (MB/s)						
	100	200	300	400	500	600	700
4096	1.176x	1.065x	1.085x	1.189x	1.127x	1.213x	1.221x
8192	1.156x	1.086x	1.126x	1.132x	1.175x	1.305x	1.166x
16384	1.180x	1.113x	1.190x	1.237x	1.219x	1.334x	1.147x
32768	1.189x	1.159x	1.225x	1.354x	1.418x	1.238x	1.077x
65536	1.240x	1.161x	1.223x	1.275x	1.153x	1.124x	0.915x

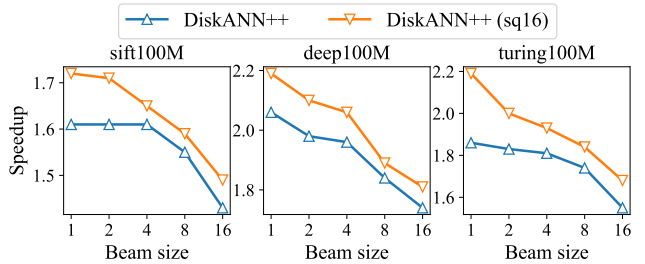


Figure 9: Effect of beamsize B on speedup.

in fewer unprocessed data blocks in page heap can be used for page expansion. However, as mentioned in the original DiskANN paper, continuously increasing the beam size is not conducive to load balancing for SSD across different queries (the original paper suggests $B = 2, 4, 8$ for better performance). Therefore, under such parameter settings, DiskANN++ still exhibits at least 1.5x speedup.

7 RELATED WORK

We review the technologies relevant to our research, including ANNS especially graph-based ANNS, and DiskANN and its variants.

Approximate nearest neighbor search (ANNS). The researches of ANNS can be generally categorized as three types: quantization-based [20, 32, 33, 39, 51], hash-based [21, 23, 26, 34, 55, 57], and graph-based [18, 19, 25, 37, 38] ANNS. Among them, graph-based methods achieve a favorable tradeoff between accuracy and efficiency by employing offline constructed nearest neighbor graph as a index and performing online heuristic search on this index [5, 8, 24, 52]. However, existing research has primarily focused on optimizing search accuracy and efficiency but ignore the significant memory overhead for maintaining the index of large-scale dataset. This motivates the following disk-resident graph-based ANNS.

Disk-resident graph-based ANNS. Most of the solutions are based on hybrid indexing schemes that utilize both disk and memory. GRIP [64] reduces the memory consumption of a graph index by compressing high-dimensional vectors to lower-dimensional ones. HM-ANN [43] addresses memory challenges through heterogeneous storage solutions. SPANN [11] is a partition tree-based method that maintains a small SPT in memory but the full vectors in disk. BBANN [47] combines an memory resident invert index and on-disk graph index to optimize range search tasks effectively. The search accuracy of above methods is affected by the compressed vectors, low-quality invert index and SPT, resulting in a noticeable accuracy loss. So, researchers resort to DiskANN family of methods to reduce memory overhead while ensuring a high accuracy.

DiskANN family of methods. DiskANN [29] introduces product quantization to assist graph-based search and significantly reduced memory usage. DiskANN has been widely deployed in the industry

such as Bing search of Microsoft [63] and many follow-up works present variants of DiskANN to support their own scenarios, e.g., Filter-DiskANN for filtered search [22], OOD-DiskANN for cross-modal search [28], and Fresh-DiskANN for streaming search [48]. Although DiskANN and its variants achieve a good performance on both memory overhead and search accuracy, they all ignore the fact that frequent frequent SSD I/O requests would significantly affect the overall QPS. This motivates our research in this paper, that is to address the I/O issue of DiskANN while retaining its strengths.

8 CONCLUSION

This paper proposes DiskANN++ that consists of three novel optimizations for DiskANN. (1) It expedites the convergence of graph search to the query neighborhood by employing query-sensitive entry vertex. (2) It applies isomorphic mapping on SSD-resident Vamana to refine its SSD layout and enhance each SSD page's data value. (3) It replaces original beamsearch by a new pagedsearch based on the refined SSD layout with an asynchronous page expansion, thus speeding up search convergence and reducing SSD I/O requests. Experimental results demonstrate that DiskANN++ achieves state-of-the-art performance compared to popular disk-based algorithms and provides a stable speedup over DiskANN across various hardware configurations and datasets.

ACKNOWLEDGMENTS

This work was supported by the National NSF of China (62072149), the Primary R&D Plan of Zhejiang (2023C03198 and 2021C03156), and the Fundamental Research Funds for the Provincial Universities of Zhejiang (GK219909299001-006).

REFERENCES

- [1] David Adedayo Adeniyi, Zhaoqiang Wei, and Yang Yongquan. 2016. Automated web usage data mining and recommendation system using K-Nearest Neighbor (KNN) classification method. *Applied Computing and Informatics* 12, 1 (2016), 90–108.
- [2] Anon. 2010. *Datasets for approximate nearest neighbor search*. Retrieved October 05, 2020 from <http://corpus-texmex.irisa.fr/>
- [3] Anon. 2011. *Million Song Dataset Benchmarks*. Retrieved April 15, 2020 from <http://www.ifs.tuwien.ac.at/mir/msd/>
- [4] Anon. unknown. *Common Crawl*. Retrieved April 15, 2020 from <http://commoncrawl.org/>
- [5] Kazuo Aoyama, Atsunori Ogawa, Takashi Hattori, Takaaki Hori, and Atsushi Nakamura. 2013. Graph index based query-by-example search on a large speech data set. In *2013 IEEE International Conference on Acoustics, Speech and Signal Processing*. IEEE, 8520–8524.
- [6] Akhil Arora, Sakshi Sinha, Piyush Kumar, and Arnab Bhattacharya. 2018. HD-Index: Pushing the Scalability-Accuracy Boundary for Approximate kNN Search in High-Dimensional Spaces. *Proceedings of the VLDB Endowment* 11, 8 (2018).
- [7] Sunil Arya and David M Mount. 1993. Approximate nearest neighbor queries in fixed dimensions.. In *SODA*, Vol. 93. 271–280.
- [8] Martin Aumüller, Erik Bernhardsson, and Alexander Faithfull. 2020. ANN-Benchmarks: A benchmarking tool for approximate nearest neighbor algorithms. *Information Systems* 87 (2020), 101374.
- [9] Maxim Babenko and Alexey Gusakov. 2011. New Exact and Approximation Algorithms for the Star Packing Problem in Undirected Graphs. *Symposium on Theoretical Aspects of Computer Science (STACS2011)* 9 (03 2011). <https://doi.org/10.4230/LIPIcs.STACS.2011.519>
- [10] Vishwanath Bjalwan, Vinay Kumar, Pinki Kumari, and Jordan Pascual. 2014. KNN based machine learning approach for text and document mining. *International Journal of Database Theory and Application* 7, 1 (2014), 61–70.
- [11] Qi Chen, Bing Zhao, Haidong Wang, Mingjin Li, Chuanjie Liu, Zengzhong Li, Mao Yang, and Jingdong Wang. 2021. SPANN: Highly-efficient Billion-scale Approximate Nearest Neighborhood Search. *Advances in Neural Information Processing Systems* 34 (2021), 5199–5212.
- [12] Chih-Yi Chiu, Amorntip Prayoonwong, and Yin-Chih Liao. 2019. Learning to index for nearest neighbor search. *IEEE transactions on pattern analysis and machine intelligence* 42, 8 (2019), 1942–1956.
- [13] Thomas Cover and Peter Hart. 1967. Nearest neighbor pattern classification. *IEEE transactions on information theory* 13, 1 (1967), 21–27.
- [14] D.W. Dearholt, N. Gonzales, and G. Kurup. 1988. Monotonic Search Networks For Computer Vision Databases, Vol. 2. 548–553. <https://doi.org/10.1109/ACSSC.1988.754602>
- [15] Elena Facco, Maria d'Errico, Alex Rodriguez, and Alessandro Laio. 2017. Estimating the intrinsic dimension of datasets by a minimal neighborhood information. *Scientific Reports* 7 (09 2017). <https://doi.org/10.1038/s41598-017-11873-y>
- [16] Miroslav Fiedler. 1973. Algebraic connectivity of graphs. *Czechoslovak Mathematical Journal* 23 (1973), 298–305. <https://api.semanticscholar.org/CorpusID:117770486>
- [17] Myron Flickr, Harpreet Sawhney, Wayne Niblack, Jonathan Ashley, Qian Huang, Byron Dom, Monika Gorkani, Jim Hafner, Denis Lee, Dragutin Petkovic, et al. 1995. Query by image and video content: The QBIC system. *computer* 28, 9 (1995), 23–32.
- [18] Cong Fu and Deng Cai. 2016. EFANNA : An Extremely Fast Approximate Nearest Neighbor Search Algorithm Based on kNN Graph. (09 2016).
- [19] Cong Fu, Chao Xiang, Changxu Wang, and Deng Cai. 2017. Fast approximate nearest neighbor search with the navigating spreading-out graph. *arXiv preprint arXiv:1707.00143* (2017).
- [20] Tiezheng Ge, Kaiming He, Qifa Ke, and Jian Sun. 2013. Optimized product quantization for approximate nearest neighbor search. In *Proceedings of the IEEE Conference on Computer Vision and Pattern Recognition*. 2946–2953.
- [21] Aristides Gionis, Piotr Indyk, Rajeev Motwani, et al. 1999. Similarity search in high dimensions via hashing. In *VLDB*, Vol. 99. 518–529.
- [22] Siddharth Gollapudi, Neel Karia, Varun Sivashankar, Ravishankar Krishnaswamy, Nikit Begwani, Swapnil Raz, Yiyong Lin, Yin Zhang, Neelam Mahapatro, Premkumar Srinivasan, Amit Singh, and Harsha Vardhan Simhadri. 2023. Filtered-DiskANN: Graph Algorithms for Approximate Nearest Neighbor Search with Filters. In *Proceedings of the ACM Web Conference 2023*. 3406–3416.
- [23] Long Gong, Huayi Wang, Mitsunori Ogihara, and Jun Xu. 2020. iDEC: indexable distance estimating codes for approximate nearest neighbor search. *Proceedings of the VLDB Endowment* 13, 9 (2020).
- [24] Hakim Hacid and Tetsuya Yoshida. 2010. Neighborhood graphs for indexing and retrieving multi-dimensional data. *Journal of Intelligent Information Systems* 34 (2010), 93–111.
- [25] Kiana Hajebi, Yasin Abbasi-Yadkori, Hossein Shahbazi, and Hong Zhang. 2011. Fast approximate nearest-neighbor search with k-nearest neighbor graph. In *Twenty-Second International Joint Conference on Artificial Intelligence*.
- [26] Qiang Huang, Jianlin Feng, Qiong Fang, Wilfred Ng, and Wei Wang. 2017. Query-aware locality-sensitive hashing scheme for lp norm. *The VLDB Journal* 26, 5 (2017), 683–708.
- [27] Piotr Indyk and Rajeev Motwani. 1998. Approximate nearest neighbors: towards removing theeff curse of dimensionality. In *Proceedings of the thirtieth annual ACM symposium on Theory of computing*. 604–613.
- [28] Shikhar Jaiswal, Ravishankar Krishnaswamy, Ankit Garg, Harsha Vardhan Simhadri, and Sheshansh Agrawal. 2022. OOD-DiskANN: Efficient and Scalable Graph ANNS for Out-of-Distribution Queries. *arXiv preprint arXiv:2211.12850* (2022).
- [29] Suhas Jayaram Subramanya, Fnu Devvrit, Harsha Vardhan Simhadri, Ravishankar Krishnaswamy, and Rohan Kadekodi. 2019. Diskann: Fast accurate billion-point nearest neighbor search on a single node. *Advances in Neural Information Processing Systems* 32 (2019).
- [30] Pennington Jeffrey, Socher Richard, and D. Manning Christopher. 2015. *GloVe: Global Vectors for Word Representation*. Retrieved April 15, 2020 from <http://nlp.stanford.edu/projects/glove/>
- [31] Herve Jegou, Matthijs Douze, and Cordelia Schmid. 2010. Product quantization for nearest neighbor search. *IEEE transactions on pattern analysis and machine intelligence* 33, 1 (2010), 117–128.
- [32] Herve Jegou, Matthijs Douze, and Cordelia Schmid. 2011. Product Quantization for Nearest Neighbor Search. *IEEE transactions on pattern analysis and machine intelligence* 33 (01 2011), 117–28. <https://doi.org/10.1109/TPAMI.2010.57>
- [33] Yannis Kalantidis and Yannis Avrithis. 2014. Locally Optimized Product Quantization for Approximate Nearest Neighbor Search. In *CVPR* (01 2014), 2321–2328.
- [34] Svebor Karaman, Xudong Lin, Xuefeng Hu, and Shih-Fu Chang. 2019. Unsupervised rank-preserving hashing for large-scale image retrieval. In *Proceedings of the 2019 on International Conference on Multimedia Retrieval*. 192–196.
- [35] George Karypis, Vipin Kumar, and Siam Comput. 1970. A Fast And High Quality Multilevel Scheme For Partitioning Irregular Graphs. *SIAM Journal on Scientific Computing* 20 (02 1970).
- [36] Wen Li, Ying Zhang, Yifang Sun, Wei Wang, Mingjie Li, Wenjie Zhang, and Xuemin Lin. 2019. Approximate nearest neighbor search on high dimensional data—experiments, analyses, and improvement. *IEEE Transactions on Knowledge and Data Engineering* 32, 8 (2019), 1475–1488.
- [37] Yury Malkov, Alexander Ponomarenko, Andrey Logvinov, and Vladimir Krylov. 2014. Approximate nearest neighbor algorithm based on navigable small world graphs. *Information Systems* 45 (2014), 61–68.

[38] Yu Malkov and Dmitry Yashunin. 2016. Efficient and Robust Approximate Nearest Neighbor Search Using Hierarchical Navigable Small World Graphs. *IEEE Transactions on Pattern Analysis and Machine Intelligence* PP, 4 (03 2016), 824–836. <https://doi.org/10.1109/TPAMI.2018.2889473>

[39] Zhibin Pan, Liangzhuang Wang, Yang Wang, and Yuchen Liu. 2020. Product Quantization with Dual Codebooks for approximate Nearest Neighbor Search. *Neurocomputing* 401 (03 2020). <https://doi.org/10.1016/j.neucom.2020.03.016>

[40] Rodrigo Paredes and Edgar Chávez. 2005. Using the k-nearest neighbor graph for proximity searching in metric spaces. In *String Processing and Information Retrieval: 12th International Conference, SPIRE 2005, Buenos Aires, Argentina, November 2-4, 2005. Proceedings* 12. Springer, 127–138.

[41] Kai Peng and Qingjia Huang. 2018. Clustering Approach Based on Mini Batch Kmeans for Intrusion Detection System Over Big Data. *IEEE Access* PP (02 2018), 1–1. <https://doi.org/10.1109/ACCESS.2018.2810267>

[42] Fabio Petroni, Leonardo Querzoni, Khuzaima Daudjee, Shahin Kamali, and Giorgio Iacoboni. 2015. HDRF: Stream-Based Partitioning for Power-Law Graphs. 243–252. <https://doi.org/10.1145/2806416.2806424>

[43] Jie Ren, Minjia Zhang, and Dong Li. 2020. Hm-ann: Efficient billion-point nearest neighbor search on heterogeneous memory. *Advances in Neural Information Processing Systems* 33 (2020), 10672–10684.

[44] Badrul Sarwar, George Karypis, Joseph Konstan, and John Riedl. 2001. Item-based collaborative filtering recommendation algorithms. In *Proceedings of the 10th international conference on World Wide Web*. 285–295.

[45] Larissa C Shimomura, Rafael Seidi Oyamada, Marcos R Vieira, and Daniel S Kaster. 2021. A survey on graph-based methods for similarity searches in metric spaces. *Information Systems* 95 (2021), 101507.

[46] Chanop Silpa-Anan and Richard Hartley. 2008. Optimised KD-trees for fast image descriptor matching. In *2008 IEEE Conference on Computer Vision and Pattern Recognition*. IEEE, 1–8.

[47] Harsha Simhadri, George Williams, Martin Aumüller, Matthijs Douze, Artem Babenko, Dmitry Baranchuk, Qi Chen, Lucas Hosseini, Ravishankar Krishnaswamy, Gopal Srinivasa, Suhas Subramanya, and Jingdong Wang. 2022. Results of the NeurIPS’21 Challenge on Billion-Scale Approximate Nearest Neighbor Search. (05 2022).

[48] Aditi Singh, Suhas Jayaram Subramanya, Ravishankar Krishnaswamy, and Harsha Vardhan Simhadri. 2021. FreshDiskANN: A Fast and Accurate Graph-Based ANN Index for Streaming Similarity Search. *arXiv preprint arXiv:2105.09613* (2021).

[49] Isabelle Stanton and Gabriel Kliot. 2012. Streaming Graph Partitioning for Large Distributed Graphs. *Proceedings of the ACM SIGKDD International Conference on Knowledge Discovery and Data Mining*. <https://doi.org/10.1145/2339530.2339722>

[50] Charalampos Tsourakakis, Christos Gkantsidis, Bozidar Radunovic, and Milan Vojnovic. 2014. FENNEL: Streaming graph partitioning for massive scale graphs. *WSDM 2014 - Proceedings of the 7th ACM International Conference on Web Search and Data Mining*, 333–342. <https://doi.org/10.1145/2556195.2556213>

[51] Jingdong Wang and Ting Zhang. 2017. Composite Quantization. *IEEE Transactions on Pattern Analysis and Machine Intelligence* PP (12 2017). <https://doi.org/10.1109/TPAMI.2018.2835468>

[52] Mengzhao Wang, Xiaoliang Xu, Qiang Yue, and Yuxiang Wang. 2021. A comprehensive survey and experimental comparison of graph-based approximate nearest neighbor search. *Proceedings of the VLDB Endowment* 14 (07 2021), 1964–1978. <https://doi.org/10.14778/3476249.3476255>

[53] Qinyong Wang, Hongzhi Yin, Tong Chen, Junliang Yu, Alexander Zhou, and Xiangliang Zhang. 2022. Fast-adapting and privacy-preserving federated recommender system. *The VLDB Journal* 31, 5 (2022), 877–896.

[54] Hao Wei, Jeffrey Yu, Can Lu, and Xuemin Lin. 2016. Speedup Graph Processing by Graph Ordering. 1813–1828. <https://doi.org/10.1145/2882903.2915220>

[55] Yair Weiss, Antonio Torralba, and Rob Fergus. 2008. Spectral Hashing. In *Advances in Neural Information Processing Systems*, D. Koller, D. Schuurmans, Y. Bengio, and L. Bottou (Eds.), Vol. 21. Curran Associates, Inc. https://proceedings.neurips.cc/paper_files/paper/2008/file/d58072be2820e8682c0a27c0518e805e-Paper.pdf

[56] Cong Xie, L. Yan, W.-J Li, and Z. Zhang. 2014. Distributed power-law graph computing: Theoretical and empirical analysis. *Advances in Neural Information Processing Systems* 2 (01 2014), 1673–1681.

[57] Hao Xu, Jingdong Wang, Zhu Li, Gang Zeng, Shipeng Li, and Nenghai Yu. 2011. Complementary hashing for approximate nearest neighbor search. 1631–1638. <https://doi.org/10.1109/ICCV.2011.6126424>

[58] Xiaoliang Xu, Jun Liu, Yuxiang Wang, and Xiangyu Ke. 2022. Academic Expert Finding via (k, P) -Core based Embedding over Heterogeneous Graphs. In *2022 IEEE 38th International Conference on Data Engineering (ICDE)*. IEEE, 338–351.

[59] Xiaoliang Xu, Mengzhao Wang, Yuxiang Wang, and Dingcheng Ma. 2021. Two-stage routing with optimized guided search and greedy algorithm on proximity graph. *Knowledge-Based Systems* 229 (07 2021), 107305. <https://doi.org/10.1016/j.knosys.2021.107305>

[60] Artem Yandex and Victor Lempitsky. 2016. Efficient Indexing of Billion-Scale Datasets of Deep Descriptors. 2055–2063. <https://doi.org/10.1109/CVPR.2016.226>

[61] Chenzi Zhang, Fan Wei, Qin Liu, Zhihao Tang, and Zhenguo Li. 2017. Graph Edge Partitioning via Neighborhood Heuristic. 605–614. <https://doi.org/10.1145/3097983.3098033>

[62] Hongfei Zhang, Xia Song, Chenyan Xiong, Corby Rosset, Paul Bennett, Nick Craswell, and Saurabh Tiwary. 2019. Generic Intent Representation in Web Search. 65–74. <https://doi.org/10.1145/3331184.3331198>

[63] Jianjin Zhang, Zheng Liu, Weihao Han, Shitao Xiao, Ruicheng Zheng, Yingxia Shao, Hao Sun, Hanqing Zhu, Premkumar Srinivasan, Weiwei Deng, Qi Zhang, and Xing Xie. 2022. Uni-Retriever: Towards Learning the Unified Embedding Based Retriever in Bing Sponsored Search. In *KDD*. 4493–4501.

[64] Minjia Zhang and Yuxiong He. 2019. GRIP: Multi-Store Capacity-Optimized High-Performance Nearest Neighbor Search for Vector Search Engine. In *Proceedings of the 28th ACM International Conference on Information and Knowledge Management*. 1673–1682. <https://doi.org/10.1145/3357384.3357938>

[65] Chun Jiang Zhu, Tai Zhu, Haining Li, Jinbo Bi, and Minghu Song. 2019. Accelerating large-scale molecular similarity search through exploiting high performance computing. In *2019 IEEE International Conference on Bioinformatics and Biomedicine (BIBM)*. IEEE, 330–333.

[66] Dantong Zhu and Minjia Zhang. 2021. Understanding and Generalizing Monotonic Proximity Graphs for Approximate Nearest Neighbor Search. *arXiv preprint arXiv:2107.13052* (2021).